

# Bayesian uncertainty quantification of turbulence models based on high-order adjoint

Dimitrios I. Papadimitriou, Costas Papadimitriou\*

Department of Mechanical Engineering, University of Thessaly, Pedion Areos, Volos 38334, Greece



## ARTICLE INFO

### Article history:

Received 9 October 2014

Revised 9 July 2015

Accepted 16 July 2015

Available online 31 July 2015

### Keywords:

Bayesian inference

Uncertainty quantification

Parameter estimation

Turbulence modeling

Adjoint methods

## ABSTRACT

The uncertainties in the parameters of turbulence models employed in computational fluid dynamics simulations are quantified using the Bayesian inference framework and analytical approximations. The posterior distribution of the parameters is approximated by a Gaussian distribution with the most probable value obtained by minimizing the objective function defined by the minus of the logarithm of the posterior distribution. The gradient and the Hessian of the objective function with respect to the parameters are computed using the direct differentiation and the adjoint approach to the flow equations including the turbulence model ones. The Hessian matrix is used both to compute the covariance matrix of the posterior distribution and to initialize the quasi-Newton optimization algorithm used to minimize the objective function. The propagation of uncertainties in output quantities of interest is also presented based on Laplace asymptotic approximations and the adjoint formulation. The proposed method is demonstrated using the Spalart–Allmaras turbulence model parameters in the case of the flat plate flow using DNS data for velocities and the flow through a backward facing step using experimental data for velocities and Reynolds stresses.

© 2015 Elsevier Ltd. All rights reserved.

## 1. Introduction

The Bayesian inference method for the quantification and propagation of the uncertainties in computational models has been developed and widely used in the scientific community. The method aims at the selection among alternative plausible model structures to represent physical phenomenon and the unmodelled dynamics, estimation of the uncertainties in the parameters of these model structures, as well as propagation of uncertainties through the model to make robust predictions of output quantities of interest (QoI), consistent with available experimental measurements. There are several scientific areas the Bayesian method has been applied such as structural dynamics [1–5], molecular dynamics [6], heat conduction [7], flight dynamics [8,9], bioengineering [10], computational fluid dynamics (CFD) [11–13] and aeroelasticity [14].

The Bayesian tools are analytical asymptotic approximations [5,15,16,18,19] and stochastic simulation algorithms such as variants of Markov Chain Monte Carlo [20–24]. In particular, the analytical tools involve solving optimization problems and computing the Hessian of objective functions that involve model-based output QoI. Analytical techniques have computational advantages since they require a moderate number of system re-analyses in comparison to

the very large number of system re-analyses needed in the stochastic simulation algorithms. However, analytical techniques are model intrusive, requiring extensive analytical developments of first and second-order derivatives and extensive numerical implementation in available system simulation software. In contrast, stochastic simulation algorithms are in general model non-intrusive, avoiding the cumbersome procedure for calculating gradients. In addition, surrogate models can be integrated in stochastic simulation algorithms to reduce the computational effort [25,26]. In this work, analytical approximations are employed for Bayesian uncertainty quantification and propagation of turbulence models used in CFD simulations. Direct differentiation and higher-order adjoint formulations are developed to address computational issues associated with the optimization problems and compute the Hessian matrices involved in the Bayesian analytical approximations.

The adjoint approach has proved to be a very powerful tool in control theory for deterministic optimization problems, providing inexpensively the derivatives of the objective function with respect to the control variables. The first adjoint approach [27] attempted to handle an optimization problem as a control problem while the application of the adjoint approach to the optimization of CFD problems was introduced in [28,29] for potential flows and extended later to transonic inviscid flows [30–32] and viscous flows, [33]. Several improvements and extensions of the adjoint approach can also be found in the literature [34–38], all of which are related to the computation of first order sensitivity derivatives

\* Corresponding author. Tel.: +30 242 107 4006.

E-mail addresses: [dpapadim@uth.gr](mailto:dpapadim@uth.gr) (D.I. Papadimitriou), [costasp@uth.gr](mailto:costasp@uth.gr) (C. Papadimitriou).

using the adjoint approach and their application to optimization in CFD.

Concerning the adjoint approach for the computation of higher order derivatives the literature is scarce. Second-order sensitivity analysis for CFD optimization using the discrete adjoint has been based on automatic differentiation [39] or hand differentiation [40,41], while the corresponding continuous approach has been presented in [42] for inviscid and in [43,44] for viscous flows. The extension to third-order sensitivity analysis for robust design using the method of moments is presented in [45,46]. The second-order sensitivity analysis can also be met in other disciplines than aerodynamics such as structural mechanics [47], heat conduction problems [48] and meteorology [49].

As far as the differentiation of turbulence models is concerned, the  $k-\epsilon$  turbulence model with wall functions has been differentiated in [50–52], aiming at the computation of the sensitivity derivatives of QoI with respect to the turbulence model parameters. Also, the discrete adjoint approach to turbulence modeling has been presented in [53] while its continuous counterpart has been developed for the efficient optimization of turbulent flows, modelled using low Reynolds turbulence models [54,55] or high Reynolds models with wall functions [55].

In this paper, the uncertainties in the parameters of turbulence models employed in CFD simulations are quantified by the posterior distribution of the model parameters using the Bayesian inference framework. Using analytical approximations, the posterior distribution is represented by a Gaussian distribution which is centered at the most probable value of the model parameters. This value is obtained by minimizing the objective function defined by the minus of the logarithm of the posterior distribution. The covariance matrix of the posterior Gaussian distribution is obtained as the inverse of the Hessian of the objective function evaluated at the most probable value.

The present work complements recent developments [11,12] on Bayesian inference methods for parameter estimation of turbulence models based on alternative stochastic simulation algorithms, such as variants of MCMC, and applied on flow over a flat plate using velocity and friction coefficient profile measurements. Another related work may be found in [56], which attempts to shed light in the epistemic uncertainties of RANS turbulence model without, however, quantifying their parameters using an inverse approach. Also, in [57], the uncertainties of the  $k-\omega$  RANS turbulence model are quantified using the adjoint approach, by finding the turbulence viscosity distribution that produces a flow field as close as possible to the one computed by DNS simulations in a duct.

The adjoint approach is developed to compute the gradient of the objective function with respect to the turbulence model parameters and a quasi-Newton algorithm is used to find the most probable solution. The Hessian matrix of the second-order sensitivities of the objective function with respect to the turbulence model parameters is used to initialize the quasi-Newton algorithm to improve the convergence of the optimization algorithm and to compute the covariance matrix of the posterior distribution. It is computed using the so-called direct-adjoint approach which is the most efficient combination of the direct-differentiation and the adjoint approach, whose cost scales to the number of design variables. The multi-dimensional probability integrals that arise in the propagation of uncertainties in various output QoI are also computed using Laplace asymptotic approximations that involve appropriate objective function derivatives and Hessians.

The present work is organized as follows. Section 2 presents the Bayesian framework and the analytical asymptotic approximations for uncertainty quantification and propagation. Sections 3, 4 and 5 apply the Bayesian formulation to CFD problems and develop the general expressions for the first and second-order adjoint techniques. For demonstration purposes, the proposed method is applied to the estimation of the Spalart–Allmaras turbulence model parameters. The methodology is demonstrated in Section 6 by estimating the param-

eters of the Spalart–Allmaras turbulence model as well as propagating uncertainties in output QoIs for two well-known cases: the flat plate flow using DNS axial velocities instead of experimental values and the flow through a backward facing step using experimental values of the axial velocity and Reynolds shear stress profiles at five longitudinal positions. In particular, the effect of spatially correlated and uncorrelated prediction error models is investigated. Section 7 summarizes the main conclusions of this study.

## 2. Bayesian framework and asymptotic analysis

Assume that a CFD model (i.e. a RANS model described by the mean flow and turbulence model equations) is used to predict a quantity of interest (QoI) (such as the drag or lift of an airfoil/wing or the total pressure losses in a duct or a turbomachinery cascade) in a flow test case. Let  $\theta^p \in \mathbb{R}^{N_{\theta p}}$  represent the vector of parameters of the CFD model, such as the parameters involved in a turbulence model, whose values are to be estimated based on experimental data. Let  $\underline{d} \in \mathbb{R}^N$  be the vector of measured data of flow quantities available from experiments (such as velocities, Reynolds stresses, pressure coefficients, friction coefficients, etc.) and  $\underline{y}(\theta^p) \in \mathbb{R}^N$  be the vector of the values of the same quantities computed by the model for specific values of  $\theta^p$ .

### 2.1. Uncertainty quantification and estimation

The objective is to quantify the uncertainty in the parameters  $\theta^p$  and model the missing (incomplete) information provided by the selected flow model given the experimental data, as well as to propagate these uncertainties through the flow model to predict the uncertainties in output QoI. Probability density functions (PDF) are used to quantify uncertainties and the calculus of probability is employed for handling and propagating uncertainties through the model in a consistent manner. To model the incomplete information due to the selection of a particular flow model, a probabilistic model is built to characterize the deviation between the experimental and the model predicted values. For this, the measured data and the corresponding model predictions satisfy the prediction error equation

$$\underline{d} = \underline{y}(\theta^p) + \underline{e} \quad (1)$$

where  $\underline{e}$  is the prediction error due to the measurement, computational and modeling uncertainties. Assuming that the prediction error is characterized by a zero-mean and a covariance  $\Sigma$ , the principle of maximum entropy is invoked to model the prediction error by a Gaussian vector. It is assumed that the structure of the covariance matrix depends on a parameter set  $\theta^e$ , ( $\Sigma \equiv \Sigma(\theta^e) \in \mathbb{R}^{N \times N}$ ). The parameters  $\theta^e$  are estimated jointly with  $\theta^p$ , based on the experimental measurements.

Alternative mixed multiplicative/additive prediction error models have been introduced in [11] to satisfy the no-slip boundary condition at wall surfaces. The no-slip boundary conditions can be taken into account in the additive prediction error term, Eq. (1), by letting the  $i$ th component of  $\underline{e}$  to be  $e_i = \epsilon_i \bar{d}_i$ , where  $\bar{d}_i$  is the mean experimental value of the  $i$ th measurement and  $\epsilon_i$  is the  $i$ th element of the Gaussian vector  $\underline{\epsilon}$ , i.e. the prediction error term due to modeling error is taken to be proportional to the  $i$ th experimental value. These alternative formulations for the prediction error terms can readily be integrated within the proposed Bayesian framework.

Note that an unbiased model error is assumed in Eq. (1). However, the model error is not expected to be unbiased. Biased model errors have been proposed in [58]. In this work, the use of a zero-mean assumption for the model error is a compromise between probabilistic modelling and the need to limit the number of parameters for inference.

Following a Bayesian formulation [5], the posterior PDF of the combined parameter set  $\underline{\theta} = (\theta^p, \theta^e)$  given the measured data  $\underline{d}$ , is

given by

$$p(\underline{\theta}|\underline{d}) = \frac{p(\underline{d}|\underline{\theta})\pi(\underline{\theta})}{p(\underline{d})} \quad (2)$$

where  $p(\underline{d}|\underline{\theta})$  is the *likelihood* of observing the data  $\underline{d}$  from the model for given values of the parameters  $\underline{\theta}$ ,  $\pi(\underline{\theta})$  is the *prior* probability of the parameters  $\underline{\theta}$ , and  $p(\underline{d})$  is the *evidence* of the model class given by

$$p(\underline{d}) = \int p(\underline{d}|\underline{\theta})\pi(\underline{\theta})d\underline{\theta} \quad (3)$$

so that the posterior PDF integrates to one. Using the Gaussian model for the prediction error  $\underline{e}$ , the likelihood function is given by

$$p(\underline{d}|\underline{\theta}) = \frac{1}{(2\pi)^{\frac{N_d}{2}} \det \Sigma^{\frac{1}{2}}} \exp\left[-\frac{1}{2}J(\underline{\theta}; \underline{d})\right] \quad (4)$$

where

$$J(\underline{\theta}; \underline{d}) = [\underline{d} - \underline{y}(\underline{\theta}^p)]^T \Sigma(\underline{\theta}^e)^{-1} [\underline{d} - \underline{y}(\underline{\theta}^p)] \quad (5)$$

expresses the deviation between the measured and model predicted quantities.

Using a well-established analytical approximation, valid for large number of experimental data, the posterior distribution of the model parameters can be approximated by a multi-variable Gaussian distribution

$$\begin{aligned} p(\underline{\theta}|\underline{d}) &\sim p_a(\underline{\theta}|\underline{d}) \\ &= \frac{1}{(2\pi)^{\frac{N_\theta}{2}} \det H^{-\frac{1}{2}}} \exp\left[-\frac{1}{2}(\underline{\theta} - \hat{\underline{\theta}})^T H(\hat{\underline{\theta}})(\underline{\theta} - \hat{\underline{\theta}})\right] \end{aligned} \quad (6)$$

centered at the most probable value  $\hat{\underline{\theta}}$  of the posterior distribution function or equivalently the minimum of the function

$$L(\underline{\theta}) = -\log(p(\underline{d}|\underline{\theta})\pi(\underline{\theta})) \quad (7)$$

given by

$$\hat{\underline{\theta}} = \arg \min_{\underline{\theta}} [L(\underline{\theta})] \quad (8)$$

and with covariance  $C(\hat{\underline{\theta}})$  equal to the inverse of the Hessian  $H(\hat{\underline{\theta}})$  of the function  $L(\underline{\theta})$  estimated at the most probable value  $\hat{\underline{\theta}}$ . The uncertainty in  $\underline{\theta}$  can thus be fully described asymptotically by solving an optimization problem for finding the most probable value  $\hat{\underline{\theta}}$  that minimizes the function  $L(\underline{\theta})$ , and also evaluating the Hessian of the function  $L(\underline{\theta})$  at a single point  $\hat{\underline{\theta}}$ . Herein it is assumed that only one global optimum exists with probability volume that dominates the ones corresponding to multiple local optima. The analysis can be extended to account for more than one global/local optima with comparable probability volumes contributing to the posterior PDF [5].

For non-Gaussian posterior PDFs the asymptotic Gaussian estimate, Eq. (6), provides a computationally efficient local approximation in the neighborhood of the most probable value in the parameter space. The error in the Gaussian posterior estimate is of the order of  $1/N$  [5]. The number of data required to get accurate results using the proposed method is problem dependent. Usually, the method gives acceptable approximations for problems which are identifiable [5]. For unidentifiable problems the proposed Gaussian estimate fails to adequately represent the posterior PDF along the unidentifiable manifold in the parameter space, which may extend further away from the most probable value and along directions that may not be easily predictable by local Hessian approximations at the most probable point.

However, the Gaussian estimate has certain computational and theoretical advantages. Specifically, it uses adjoint techniques to carry out the optimization and provides a computationally efficient approximation of the posterior distribution. Instead, the alternative but accurate MCMC versions sample the posterior distribution with a

much higher computational cost. Also, the eigenvalues and eigenvectors of the Hessian at the most probable value contain important information for the directions in the parameter space along which parameters are well informed or not informed based on the data. Even for large number of data, a number of model parameters may not be informed based on the selected data. Furthermore, approximate Gaussian posteriors at the component level of a system are often very convenient distributions since they can be readily integrated within various uncertainty propagation tools to perform robust design optimization of systems based on analytical formulations, instead of computationally intensive sampling techniques.

An asymptotic estimate of the evidence of the model class based on Laplace approximation of the integral (3) is given by [2,3,16,17]

$$p(\underline{d}) = \frac{(2\pi)^{\frac{N_\theta}{2}}}{[\det H(\hat{\underline{\theta}})]^{1/2}} \exp[-L(\hat{\underline{\theta}})]. \quad (9)$$

This estimate can be used for comparing competing models.

## 2.2. Uncertainty propagation

Let  $g(\underline{\theta}, \eta)$  be an output QoI for which measurements are not available. The QoI  $g(\underline{\theta}, \eta)$  can be evaluated by

$$g(\underline{\theta}, \eta) = g_m(\underline{\theta}) + \eta \quad (10)$$

where  $g_m(\underline{\theta})$  is the prediction of the QoI from the flow model and  $\eta$  is the prediction error accounting for the model error. As in the case of measured QoI  $\underline{y}(\underline{\theta}^p)$  in Eq. (1), the model error  $\eta$  can be assumed to be Gaussian with zero mean and variance  $\sigma_\eta^2$ . The uncertainty in the output QoI can be obtained by propagating the uncertainty in the parameter set  $\underline{\theta}$  through the flow model and taking into account the model error uncertainty quantified by  $\eta$ . In contrast to the case of the error term  $\underline{e}$  in Eq. (1) for which the hyper-parameters  $\underline{\theta}^e$  defining the correlation structure can be inferred from the data, the parameter  $\sigma_\eta$  cannot be estimated for all cases where data are not available. Instead, it has to be subjectively chosen to reflect the size of the model error expected for the output QoI.

The uncertainty is next described by the mean and the standard deviation of the quantity  $g(\underline{\theta}, \eta)$ . Using Eq. (10), the mean is readily computed as

$$E[g(\underline{\theta}, \eta)] = E[g_m(\underline{\theta})]. \quad (11)$$

The standard deviation is estimated through the second moment which, taking into account that  $g_m(\underline{\theta})$  and  $\eta$  are independent variables, one readily derives from Eq. (10) that

$$E[g^2(\underline{\theta}, \eta)] = E[g_m^2(\underline{\theta})] + \sigma_\eta^2. \quad (12)$$

The variance of the QoI is finally obtained from

$$\text{Var}[g(\underline{\theta}, \eta)] = \text{Var}[g_m(\underline{\theta})] + \sigma_\eta^2 \quad (13)$$

where

$$\text{Var}[g_m(\underline{\theta})] = E[g_m^2(\underline{\theta})] - \{E[g_m(\underline{\theta})]\}^2. \quad (14)$$

The posterior mean value of  $g_m(\underline{\theta})$  is given as

$$E[g_m(\underline{\theta})] = \int g_m(\underline{\theta}) p(\underline{\theta}|\underline{d}) d\underline{\theta} \quad (15)$$

and the posterior second moment is

$$E[g_m^2(\underline{\theta})] = \int g_m^2(\underline{\theta}) p(\underline{\theta}|\underline{d}) d\underline{\theta}. \quad (16)$$

Substituting the expression of the posterior PDF in Eq. (15) yields

$$E[g_m(\underline{\theta})] = \frac{\int g_m(\underline{\theta}) p(\underline{d}|\underline{\theta}) \pi(\underline{\theta}) d\underline{\theta}}{\int p(\underline{d}|\underline{\theta}) \pi(\underline{\theta}) d\underline{\theta}}. \quad (17)$$

The Laplace asymptotic estimate for the denominator is given in Eq. (9). Applying a similar asymptotic estimate for the numerator, one

readily obtains the following asymptotic estimate for the mean value of  $g_m(\underline{\theta})$  [19]

$$E[g_m(\underline{\theta})] = \exp[L(\hat{\underline{\theta}}) - L_g(\hat{\underline{\theta}}_g)] \frac{[\det H(\hat{\underline{\theta}})]^{1/2}}{[\det H_g(\hat{\underline{\theta}}_g)]^{1/2}} \quad (18)$$

where

$$\hat{\underline{\theta}}_g = \arg \min_{\underline{\theta}} [L_g(\underline{\theta})] \quad (19)$$

the function  $L_g(\underline{\theta})$  is given by

$$L_g(\underline{\theta}) = -\log(g_m(\underline{\theta})p(d|\underline{\theta})\pi(\underline{\theta})) = -\log(g_m(\underline{\theta})) + L(\underline{\theta}) \quad (20)$$

and  $H_g(\hat{\underline{\theta}}_g)$  is the Hessian matrix of the function  $L_g(\underline{\theta})$  evaluated at  $\hat{\underline{\theta}}_g$ .

Following the same procedure for the integral in Eq. (16) that gives the second moment, it can be readily shown that

$$E[g_m^2(\underline{\theta})] = \exp[L(\hat{\underline{\theta}}) - L_{g^2}(\hat{\underline{\theta}}_{g^2})] \frac{[\det H(\hat{\underline{\theta}})]^{1/2}}{[\det H_{g^2}(\hat{\underline{\theta}}_{g^2})]^{1/2}} \quad (21)$$

where

$$\hat{\underline{\theta}}_{g^2} = \arg \min_{\underline{\theta}} [L_{g^2}(\underline{\theta})] \quad (22)$$

with  $L_{g^2}(\underline{\theta})$  given by

$$L_{g^2}(\underline{\theta}) = -\log(g_m^2(\underline{\theta})p(d|\underline{\theta})\pi(\underline{\theta})) = -\log(g_m^2(\underline{\theta})) + L(\underline{\theta}) \quad (23)$$

and  $H_{g^2}(\hat{\underline{\theta}}_{g^2})$  is the Hessian of  $L_{g^2}(\underline{\theta})$  evaluated at  $\hat{\underline{\theta}}_{g^2}$ .

The mean and the standard deviation derived based on the asymptotic approximations (18) and (21) give robust prediction of the output QoI that take into account the uncertainty in the turbulence model parameters and prediction error model parameters. The computation of the mean value and variance of any output QoI  $g(\underline{\theta}, \eta)$  requires the solution of two additional optimization problems (19) and (22) and the computation of a Hessian matrix at each optimal solution. To considerably accelerate convergence to the optimal solutions of the aforementioned optimization problems, the most probable solution  $\hat{\underline{\theta}}$  in (8) can be used as starting point in both problems. A number of techniques for Hessian estimation have been proposed, e.g. [59] and [60] for Bayesian inversion. It is evident that the first and second-order adjoint methods for turbulence models in CFD are useful techniques for considerably reducing the computational effort associated with the three optimization problems (8), (19) and (22), as well as computing the Hessian of the three objective functions involved. However, it should be mentioned that the traditional MCMC approaches, though being much more costly even when metamodeling techniques are used to alleviate part of the computational burden [61], have the advantage of capturing the full histogram of the posterior distribution even for non-symmetric posteriors. Alternative second-order methods of moments [45] can be used with the Gaussian posterior distribution for uncertainty propagation. Such methods do not involve an extra optimization but their accuracy is limited to small uncertainties compared to the asymptotic estimate [62].

### 3. Flow model

The flow model consists of the 2D Navier–Stokes equations for compressible fluid flow and the Spalart–Allmaras one-equation turbulence model [63]. The mean-flow equations are written as

$$\frac{\partial U_n}{\partial t} + \frac{\partial f_{nk}^{\text{inv}}}{\partial x_k} - \frac{\partial f_{nk}^{\text{vis}}}{\partial x_k} = 0 \quad (24)$$

where, for steady flows,  $t$  is the pseudo-time and the conservative variables  $U_n$  and the inviscid  $f_{nk}^{\text{inv}}$  and viscous  $f_{nk}^{\text{vis}}$  fluxes, are

given by

$$\begin{bmatrix} U_1 \\ U_2 \\ U_3 \\ U_4 \end{bmatrix} = \begin{bmatrix} \rho \\ \rho u_1 \\ \rho u_2 \\ E \end{bmatrix}, \quad \begin{bmatrix} f_{1k}^{\text{inv}} \\ f_{2k}^{\text{inv}} \\ f_{3k}^{\text{inv}} \\ f_{4k}^{\text{inv}} \end{bmatrix} = \begin{bmatrix} \rho u_k \\ \rho u_1 u_k + p \delta_{k1} \\ \rho u_2 u_k + p \delta_{k2} \\ u_k(E + p) \end{bmatrix}, \quad (25)$$

$$\begin{bmatrix} f_{1k}^{\text{vis}} \\ f_{2k}^{\text{vis}} \\ f_{3k}^{\text{vis}} \\ f_{4k}^{\text{vis}} \end{bmatrix} = \begin{bmatrix} 0 \\ \tau_{1k} \\ \tau_{2k} \\ u_m \tau_{km} + q_k \end{bmatrix}$$

In Eq. (25),  $u_k$ ,  $E = \rho e + \frac{1}{2} \rho u_k^2$ ,  $\tau_{km} = \mu_{\text{eff}} (\frac{\partial u_k}{\partial x_m} + \frac{\partial u_m}{\partial x_k}) + \lambda \delta_{km} \frac{\partial u_l}{\partial x_l}$  and  $q_k = k \frac{\partial T}{\partial x_k}$  stand for the velocity components, total energy per unit volume, viscous stresses and heat fluxes, respectively and  $\lambda = -\frac{2}{3} \mu_{\text{eff}}$ , where  $\mu_{\text{eff}}$  is the sum of molecular and turbulent viscosities,  $\mu$  and  $\mu_t$ , respectively. Also,  $\delta_{km}$  is the Kronecker symbol.

The Spalart–Allmaras model equation for compressible flows is written as follows:

$$\frac{\partial (\rho v_k \tilde{\mu})}{\partial x_k} - \frac{1 + c_{b2}}{\sigma_{SA}} \frac{\partial}{\partial x_k} \left[ (\mu + \tilde{\mu}) \frac{\partial \tilde{\mu}}{\partial x_k} \right] + \frac{c_{b2}}{\sigma_{SA}} (\mu + \tilde{\mu}) \frac{\partial}{\partial x_k} \left( \frac{\partial \tilde{\mu}}{\partial x_k} \right) - \rho \tilde{\mu} P + \tilde{\mu} D = 0 \quad (26)$$

where  $P = c_{b1} \tilde{S}$ ,  $D = c_{w1} f_w \frac{\tilde{\mu}}{d^2}$  are the production and destruction terms, respectively,  $\tilde{\mu}$  is the turbulence state variable and  $d$  is the distance from the wall boundary. The turbulent viscosity coefficient  $\mu_t$  is written as an expression of  $\tilde{\mu}$  as follows:

$$\mu_t = \tilde{\mu} f_{v1}. \quad (27)$$

Also,

$$\chi = \frac{\tilde{\mu}}{\mu}, \quad f_{v1} = \frac{\chi^3}{\chi^3 + c_{v1}^3}, \quad f_{v2} = \frac{1}{(1 + \frac{\chi}{c_{v2}})^3},$$

$$f_{v3} = \frac{1}{\chi} (1 + \chi f_{v1}) (1 - f_{v2}) \quad (28)$$

and

$$S = \left| e_{ijk} \frac{\partial v_k}{\partial x_j} \tilde{l}_i \right|, \quad \tilde{S} = f_{v3} S + \frac{\tilde{\mu}}{\rho \kappa^2 d^2} f_{v2}$$

$$g = r + c_{w2} (r^6 - r), \quad f_w = g \left( \frac{1 + c_{w3}^6}{g^6 + c_{w3}^6} \right)^{\frac{1}{6}}, \quad r = \frac{\tilde{\mu}}{\rho \tilde{S} \kappa^2 d^2} \quad (29)$$

where  $e_{ijk}$  is the permutation symbol.

The constants which consist the parameters  $\underline{\theta}$  to be identified are  $c_{b1}$ ,  $c_{b2}$ ,  $\kappa$ ,  $\sigma_{SA}$ ,  $c_{w2}$ ,  $c_{w3}$ ,  $c_{v1}$  and  $c_{v2}$ . The nominal values for these parameters, as given in [63], are:  $\sigma_{SA} = \frac{2}{3}$ ,  $\kappa = 0.41$ ,  $c_{v1} = 7.1$ ,  $c_{v2} = 5$ ,  $c_{b1} = 0.1355$ ,  $c_{b2} = 0.622$ ,  $c_{w2} = 0.3$ ,  $c_{w3} = 2$  and  $c_{w1} = \frac{c_{b1}}{\kappa^2} + \frac{1 + c_{b2}}{\sigma_{SA}}$ .

Although the present study is based exclusively on the Spalart–Allmaras turbulence model, any other turbulence model may be used instead. The proposed first and second-order adjoint formulation is generic and can be applied in a similar manner to any other model, requiring, however, the corresponding mathematical derivations and programming.

### 4. First-order adjoint analysis

The objective function to be minimized is given in Eq. (7) which can be expressed in tensor form as

$$L = \frac{1}{2} (y_k - d_k) \Sigma_{kl}^{-1} (y_l - d_l) + \frac{1}{2} \log(\det \Sigma) + \frac{N}{2} \log(2\pi) + L_\pi \quad (30)$$

where the summation is implied for indices  $k$  and  $l$  with  $1 < k, l < N$ , the notation  $\Sigma_{kl}^{-1} \equiv [\Sigma^{-1}]_{kl}$  is used, and  $y_k$  (and  $d_k$ ) stand for the values of computed (and experimental) axial velocities ( $u_1$ ) or Reynolds



shear stresses  $\mu_t (\frac{\partial u_1}{\partial x_2} + \frac{\partial u_2}{\partial x_1})$ . The computed quantities  $y_k$  are interpolated at the locations where the experimental values are provided. The last term  $L_\pi$  is defined as

$$L_\pi \equiv L_\pi(\theta) = -\log(\pi(\theta)). \quad (31)$$

The differentiation of Eq. (30) with respect to  $\theta_i$  yields

$$\begin{aligned} \frac{dL}{d\theta_i} &= (y_k - d_k) \Sigma_{kl}^{-1} \frac{dy_l}{d\theta_i} + \frac{1}{2} (y_k - d_k) \frac{d\Sigma_{kl}^{-1}}{d\theta_i} (y_l - d_l) \\ &\quad + \frac{1}{2} \frac{d(\log(\det \Sigma))}{d\theta_i} + \frac{\partial L_\pi}{\partial \theta_i} \end{aligned} \quad (32)$$

without summation for the index  $i$ . The sensitivities of  $L$  with respect to  $\theta_i^p$  are given by

$$\frac{dL}{d\theta_i^p} = (y_k - d_k) \Sigma_{kl}^{-1} \frac{\partial y_l}{\partial U_m} \frac{dU_m}{d\theta_i^p} + \frac{\partial L_\pi}{\partial \theta_i^p} \quad (33)$$

where  $U_m = 0$  stand for the discretized mean flow and turbulence model variables ( $1 < m < N_g$ , where  $N_g$  is the number of grid nodes multiplied by 5 (the number of mean flow and turbulence model equations)).  $\frac{dL}{d\theta_i^p}$  can be computed directly by solving the equations that are derived from the direct-differentiation of the flow equations

$$\frac{dR_q}{d\theta_i^p} = \frac{\partial R_q}{\partial \theta_i^p} + \frac{\partial R_q}{\partial U_m} \frac{dU_m}{d\theta_i^p} = 0 \quad (34)$$

for  $\frac{dU_m}{d\theta_i^p}$ , where  $R_q = 0$  stand for the discretized mean flow equations, Eq. (24), and turbulence model equations, Eq. (26) ( $1 < q < N_g$ ). The total derivative symbol  $d$  is used in the term  $\frac{dU_m}{d\theta_i^p}$  instead of the partial derivative symbol  $\partial$  to emphasize on the fact that in the adjoint approach the symbol  $\partial$  is used to distinguish between  $U_m$  and  $\theta_i^p$ . The term  $\frac{\partial R_q}{\partial \theta_i^p}$  can be readily computed analytically, without incorporating significant computational cost, using Eqs. (24)–(29). Also,  $\frac{\partial R_q}{\partial U_m}$  is the Jacobian matrix of the discretized flow equations with respect to the flow variables, which can be computed directly after the flow equations are solved.

However, Eq. (34) should be solved for each parameter independently and, thus, their cost is proportional to the number of parameters  $N_{\theta p}$ . To avoid this cost, the adjoint equations are solved instead, whose cost is independent of the number of parameters. For this, the augmented objective function  $\tilde{L}$  is introduced and its sensitivity derivatives are given by

$$\frac{d\tilde{L}}{d\theta_i^p} = (y_k - d_k) \Sigma_{kl}^{-1} \frac{\partial y_l}{\partial U_m} \frac{dU_m}{d\theta_i^p} + \frac{\partial L_\pi}{\partial \theta_i^p} + \Psi_q \left( \frac{\partial R_q}{\partial \theta_i^p} + \frac{\partial R_q}{\partial U_m} \frac{dU_m}{d\theta_i^p} \right). \quad (35)$$

The terms depending on  $\frac{dU_m}{d\theta_i^p}$  are eliminated by solving the adjoint equations, given by

$$(y_k - d_k) \Sigma_{kl}^{-1} \frac{\partial y_l}{\partial U_m} + \Psi_q \frac{\partial R_q}{\partial U_m} = 0 \quad (36)$$

with a cost almost equal to the cost for solving the flow equations. After the adjoint variables  $\Psi_q$  are computed, the sensitivities  $\frac{d\tilde{L}}{d\theta_i^p}$  are computed by

$$\frac{d\tilde{L}}{d\theta_i^p} = \Psi_q \frac{\partial R_q}{\partial \theta_i^p} + \frac{\partial L_\pi}{\partial \theta_i^p}.$$

On the other hand, the sensitivities of  $L$  with respect to  $\theta_i^e$  are computed analytically by the expression

$$\frac{dL}{d\theta_i^e} = \frac{1}{2} (y_k - d_k) \frac{d\Sigma_{kl}^{-1}}{d\theta_i^e} (y_l - d_l) + \frac{1}{2} \frac{d(\log(\det \Sigma))}{d\theta_i^e} + \frac{\partial L_\pi}{\partial \theta_i^e} \quad (37)$$

where

$$\frac{d\Sigma^{-1}}{d\theta_i^e} = -\Sigma^{-1} \frac{d\Sigma}{d\theta_i^e} \Sigma^{-1} \quad (38)$$

and

$$\frac{d(\log(\det \Sigma))}{d\theta_i^e} = \text{tr} \left( \Sigma^{-1} \frac{d\Sigma}{d\theta_i^e} \right). \quad (39)$$

Finally, the sensitivities of the objective function  $L_g(\theta)$  and  $L_{g^2}(\theta)$  with respect to  $\theta_i^p$  can be computed analytically following a similar adjoint formulation that involves the output QoI  $L_g(\theta)$  and  $L_{g^2}(\theta)$  appearing in (19) and (22), respectively.

## 5. Second-order adjoint analysis

The method used to compute the Hessian matrix of the objective function  $L$  with respect to the parameters  $\theta_i$  is presented in this section. The Hessian matrix is used (a) to initialize the quasi-Newton gradient-based optimization approach instead of using the identity matrix as an initialization, accelerating the convergence to the optimum significantly and (b) to compute the posterior probability distribution of the parameters as well as the uncertainty in output QoI, based on the asymptotic approximations (6), (18) and (21).

In fact the initialization of the quasi-Newton algorithm with the exact Hessian matrix allowed to make use of a descent step size close to unity avoiding time consuming line search algorithms and avoiding a number of initial optimization cycles with (very) small step size in order to iteratively build the approximate Hessian matrix and proceed with quasi-Newton with a reasonable step size. The exactly-initialized Newton method has been demonstrated to result to better convergence characteristics in [43].

The procedure followed in this paper is the standard procedure to compute Hessian matrix components of an objective function with respect to the control parameters, similar to that of [41,64,65]. This is in fact based on the development proposed in [41], applied however for the first time in the literature to compute the second-order sensitivities of an objective function with respect to turbulence model parameters.

Among the four different approaches to compute the exact Hessian matrix, the so-called *DD – AV* approach is preferred, which is based on the direct-differentiation (*DD*) approach for the computation of first-order sensitivities and the adjoint-variable (*AV*) approach for the computation of second-order sensitivities [41,43]. Its cost is proportional to the number of parameters being equal to the cost for solving the flow equations  $N_{\theta p} + 1$  times. This cost is the lowest one comparing to the other alternatives; the cost of the *AV – DD* approach is equal to the  $2N_{\theta p} + 1$  equivalent flow solutions and that of the *DD – DD* approach scales with the square of  $N_{\theta p}$ . Just to mention that the *AV – AV* approach is transformed to either *DD – AV* or *AV – DD* and, thus, it is not considered as an additional approach.

The second-order sensitivities of  $L$  with respect to  $\theta_i^p$  are derived by differentiating Eq. (33), as follows:

$$\begin{aligned} \frac{d^2 L}{d\theta_i^p d\theta_j^p} &= (y_k - d_k) \Sigma_{kl}^{-1} \frac{\partial^2 y_l}{\partial U_m \partial U_n} \frac{dU_m}{d\theta_i^p} \frac{dU_n}{d\theta_j^p} \\ &\quad + (y_k - d_k) \Sigma_{kl}^{-1} \frac{\partial y_l}{\partial U_m} \frac{d^2 U_m}{d\theta_i^p d\theta_j^p} \\ &\quad + \Sigma_{kl}^{-1} \frac{\partial y_k}{\partial U_n} \frac{\partial y_l}{\partial U_m} \frac{dU_n}{d\theta_j^p} \frac{dU_m}{d\theta_i^p} + \frac{\partial L_\pi}{\partial \theta_i^p \partial \theta_j^p}. \end{aligned} \quad (40)$$

To compute the second term in the right hand side, the computation of  $\frac{d^2 U_m}{d\theta_i^p d\theta_j^p}$  would require the solution of the equation that is derived from the twice differentiation of the discretized flow equations, which read

$$\begin{aligned} \frac{d^2 R_q}{d\theta_i^p d\theta_j^p} &= \frac{\partial^2 R_q}{\partial \theta_i^p \partial \theta_j^p} + \frac{\partial^2 R_q}{\partial \theta_i^p \partial U_m} \frac{dU_m}{d\theta_j^p} + \frac{\partial^2 R_q}{\partial U_m \partial \theta_j^p} \frac{dU_m}{d\theta_i^p} \\ &+ \frac{\partial^2 R_q}{\partial U_m \partial U_n} \frac{dU_m}{d\theta_i^p} \frac{dU_n}{d\theta_j^p} + \frac{\partial R_q}{\partial U_m} \frac{d^2 U_m}{d\theta_i^p d\theta_j^p} = 0. \end{aligned} \quad (41)$$

This is the so-called  $DD - DD$  approach and its cost scales with  $N_{\theta^p}^2$ . Instead of solving Eq. (41) for  $\frac{d^2 U_m}{d\theta_i^p d\theta_j^p}$  the augmented function  $\tilde{L}$  is defined, whose second-order sensitivities read

$$\begin{aligned} \frac{d^2 \tilde{L}}{d\theta_i^p d\theta_j^p} &= \left( \Psi_q \frac{\partial^2 R_q}{\partial U_m \partial U_n} + (y_k - d_k) \Sigma_{kl}^{-1} \frac{\partial^2 y_l}{\partial U_m \partial U_n} + \Sigma_{kl}^{-1} \frac{\partial y_k}{\partial U_n} \frac{\partial y_l}{\partial U_m} \right) \frac{dU_m}{d\theta_i^p} \frac{dU_n}{d\theta_j^p} \\ &+ \left( \Psi_q \frac{\partial R_q}{\partial U_m} + (y_k - d_k) \Sigma_{kl}^{-1} \frac{\partial y_l}{\partial U_m} \right) \frac{d^2 U_m}{d\theta_i^p d\theta_j^p} \\ &+ \Psi_q \left( \frac{\partial^2 R_q}{\partial \theta_i^p \partial U_m} \frac{dU_m}{d\theta_j^p} + \frac{\partial^2 R_q}{\partial U_m \partial \theta_j^p} \frac{dU_m}{d\theta_i^p} \right) \\ &+ \Psi_q \frac{\partial^2 R_q}{\partial \theta_i^p \partial \theta_j^p} + \frac{\partial^2 L_\pi}{\partial \theta_i^p \partial \theta_j^p}. \end{aligned} \quad (42)$$

The second term on the right hand side is eliminated by imposing and solving the adjoint equations. These are the same as those solved for the computation of the first-order sensitivities, given by Eq. (36). The remaining terms yield the final expression for the Hessian matrix, whose computation requires, thus, the computation of  $\frac{dU_m}{d\theta_j^p}$  using the direct-differentiation of the flow equations once. The cost for this computation, as explained above, is  $N_{\theta^p}$  times the cost for the solution of the flow equations.

The derivatives  $\frac{\partial^2 R_q}{\partial U_m \partial U_n}$ ,  $\frac{\partial^2 R_q}{\partial \theta_i^p \partial U_m}$  and  $\frac{\partial^2 R_q}{\partial \theta_i^p \partial \theta_j^p}$  are also computed analytically without involving significant computational cost. Also, terms  $\frac{\partial y_k}{\partial U_n}$  and  $\frac{\partial^2 y_l}{\partial U_m \partial U_n}$  are computed analytically depending on the quantities that are measured by the experiments.

The second-order derivatives of  $L$  with respect to  $\theta^e$  are computed analytically by differentiating Eq. (37), yielding

$$\begin{aligned} \frac{d^2 L}{d\theta_i^e d\theta_j^e} &= \frac{1}{2} (y_k - d_k) \frac{d^2 \Sigma_{kl}^{-1}}{d\theta_i^e d\theta_j^e} (y_l - d_l) \\ &+ \frac{1}{2} \frac{d^2 (\log(\det \Sigma))}{d\theta_i^e d\theta_j^e} + \frac{\partial^2 L_\pi}{\partial \theta_i^e \partial \theta_j^e} \end{aligned} \quad (43)$$

where

$$\begin{aligned} \frac{d^2 \Sigma^{-1}}{d\theta_i^e d\theta_j^e} &= \Sigma^{-1} \frac{d\Sigma}{d\theta_i^e} \Sigma^{-1} \frac{d\Sigma}{d\theta_j^e} \Sigma^{-1} + \Sigma^{-1} \frac{d\Sigma}{d\theta_j^e} \Sigma^{-1} \frac{d\Sigma}{d\theta_i^e} \Sigma^{-1} \\ &- \Sigma^{-1} \frac{d^2 \Sigma}{d\theta_i^e d\theta_j^e} \Sigma^{-1} \end{aligned} \quad (44)$$

and

$$\frac{d^2 (\log(\det \Sigma))}{d\theta_i^e d\theta_j^e} = \text{tr} \left( \frac{d\Sigma^{-1}}{d\theta_i^e} \frac{d\Sigma}{d\theta_j^e} + \Sigma^{-1} \frac{d^2 \Sigma}{d\theta_i^e d\theta_j^e} \right). \quad (45)$$

The mixed derivatives of  $L$  with respect to  $\theta_i^p$  and  $\theta_j^e$  are derived by differentiating Eq. (33) with respect to  $\theta^e$

$$\frac{d^2 L}{d\theta_i^p d\theta_j^e} = (y_k - d_k) \frac{d\Sigma_{kl}^{-1}}{d\theta_j^e} \frac{\partial y_l}{\partial U_m} \frac{dU_m}{d\theta_i^p} \quad (46)$$

and they are computed using the expressions given above.

It should be mentioned that in the case of using another turbulence model, only the first and second-order partial derivatives of the discretized equations  $R_n$  with respect to the parameters  $\theta_i^p$  should be recomputed.

The proposed methodology can also be extended to 3D applications in a straightforward manner. This would require the availability of the CFD software for the flow analysis, upon which the first and second order adjoint approach could be built with no significant difficulties concerning the code development and maintenance. However, the additional computational cost would be larger due to the requirement of larger grids.

## 6. Applications

### 6.1. The flat plate flow case

#### 6.1.1. Description of flow problem

The proposed algorithm is applied to the quantification of the uncertainties of the eight parameters of the Spalart–Allmaras turbulence model and the parameters of the prediction error model in the flow over a flat plate. This flow is a well-known test case configuration for which several experiments have been conducted. Also, it has been used within Bayesian inference to validate turbulence models based on MCMC algorithms [11–13,66]. The Reynolds number based on the flat plate length is equal to  $5e + 6$  and the inlet Mach number is equal to 0.2. The calibration data are taken to be the axial velocities at the location with  $Re_\theta = 6000$ . All data used for the quantification of uncertainties are based on DNS computations [67,68]. A computational grid with 816 quadrilateral elements, obtained from [http://turbmodels.larc.nasa.gov/flatplate\\_grids.html](http://turbmodels.larc.nasa.gov/flatplate_grids.html), is used to carry out the simulations.

#### 6.1.2. Prior distributions of parameters

The estimation of uncertainty in the parameters is carried out using the Bayesian analytical approximations. Prior to the use of experimental data, the parameters are assumed to be independent. The prior distribution of the parameters are assumed to be truncated Gaussian for the turbulent model parameters and uniform for the prediction error parameters. The mean values of the Gaussian distributions are selected to be the nominal values taken from Ref. [63]. The standard deviations are selected to be 20% of the mean values. The Gaussian distributions are truncated at the tails for  $\underline{\theta} < \underline{Q}$  to avoid unrealistic negative values of the model parameters. Gaussian priors are often used to make the problem well behaved for cases for which group of parameters are not informed along certain direction in the parameter space based on the measurements. The lower bounds of the supports of the uniform distributions for the prediction error parameters are taken to be equal to zero, while the upper bounds are selected to be large enough to cover the expected range of variation of the prediction error parameters so that their value does not affect the estimation.

#### 6.1.3. Correlated and uncorrelated prediction errors

Based on the theoretical formulation, various models for the covariance matrix  $\Sigma(\theta^e)$  of prediction error model can be accommodated in the Bayesian framework. Uncorrelated models are usually assumed. However, Kennedy and O'Hagan [58] have pointed out the importance of using spatially correlated prediction error models. Papadimitriou and Lombaert [70] proposed techniques for selecting the structure of the correlation matrix among competing correlation structures. Cheung et al. [11] have used two different spatially correlated models of the prediction error for turbulence model parameter estimation. The effect of spatial correlation in the prediction errors on the uncertainty quantification and propagation is also investigated in this work by comparing two prediction error models.

The first prediction error model assumes spatially uncorrelated errors with the covariance matrix  $\Sigma_{\text{VEL}}$  for the velocity prediction errors represented in the form  $\Sigma_{\text{VEL}} = \sigma_{\text{VEL}}^2 I_{\text{VEL}}$ , where  $I_{\text{VEL}}$  is the identity matrix and  $\sigma_{\text{VEL}}$  is the constant standard deviation assumed for velocity measurements, respectively. The parameter set  $\underline{\theta}^e$  associated

**Table 1**

Flat plate: Initial and optimal parameter values and coefficients of variation (COV) using the adjoint approach for the correlated and the uncorrelated case (first six parameters).

	$\kappa$	$c_{v_1}$	$c_{v_2}$	$c_{b_1}$	$c_{b_2}$	$c_{w_2}$
Nominal value	0.410	7.100	5.000	0.1355	0.622	0.300
Optimal value (correlated)	0.422	7.674	4.833	0.1137	0.561	0.322
Optimal value (uncorrelated)	0.416	7.609	4.769	0.1097	0.544	0.329
COV (prior)	0.200	0.200	0.200	0.2000	0.200	0.200
COV (posterior, correlated)	0.044	0.072	0.200	0.0966	0.200	0.189
COV (posterior, uncorrelated)	0.039	0.065	0.200	0.0889	0.200	0.185

with the uncorrelated prediction error model is  $\underline{\theta}^e = \sigma_{\text{VEL}}$ . The second prediction error model assumes that the errors between two measurement locations are spatially correlated. The covariance matrix  $\Sigma = \Sigma_{\text{VEL}}$  is full matrix which depends on the spatial correlation structure assumed for the model errors. Herein, an exponential correlation structure is assumed so that the components  $(k, l)$  of the matrix  $\Sigma_{\text{VEL}}$  are given by

$$\Sigma_{a,kl} = \sigma_a^2 \exp\left[-\frac{\Delta_{kl}}{\lambda_a}\right] \quad (47)$$

where  $\Delta_{kl}$  is the distance between the measurement locations corresponding to the indices  $k$  and  $l$ ,  $\lambda_a$  is a measure of the spatial correlation length, and the subscript  $a$  stands, herein, for VEL. In this case the parameter set  $\underline{\theta}^e$  associated with the correlated prediction error model is  $\underline{\theta}^e = (\sigma_{\text{VEL}}, \lambda_{\text{VEL}})$ .

The derivatives of the covariance matrix  $\Sigma_a = \Sigma_{\text{VEL}}$  with respect to the parameters  $\sigma_a$  and  $\lambda_a$  required in Eqs. (38) and (39) are given by

$$\frac{\partial \Sigma_a}{\partial \sigma_a} = \frac{2}{\sigma_a} \Sigma_a, \quad \frac{\partial \Sigma_{a,kl}}{\partial \lambda_a} = \frac{\sigma_a^2}{\lambda_a^2} \Delta_{kl} \exp\left[-\frac{\Delta_{kl}}{\lambda_a}\right]. \quad (48)$$

The second derivatives also required in Eqs. (44) and (45) are given by

$$\begin{aligned} \frac{\partial^2 \Sigma_a}{\partial \sigma_a^2} &= \frac{2}{\sigma_a^2} \Sigma_a, \quad \frac{\partial^2 \Sigma_{a,kl}}{\partial \sigma_a \partial \lambda_a} = \frac{2}{\sigma_a} \frac{\partial \Sigma_{a,kl}}{\partial \lambda_a} \\ \frac{\partial^2 \Sigma_{a,kl}}{\partial \lambda_a^2} &= -2 \frac{\sigma_a^2}{\lambda_a^3} \Delta_{kl} \exp\left[-\frac{\Delta_{kl}}{\lambda_a}\right] + \frac{\sigma_a^2}{\lambda_a^4} \Delta_{kl}^2 \exp\left[-\frac{\Delta_{kl}}{\lambda_a}\right]. \end{aligned} \quad (49)$$

#### 6.1.4. Results

For the minimization of the objective function  $L(\underline{\theta})$  in Eq. (7) the SR1 quasi-Newton optimization method [71] is employed. The Hessian matrix for the initialization of the SR1 method is the exact matrix computed by the presented DD – AV approach and this led to noticeably faster convergence compared to the case that the initialization is the identity matrix.

The 64 components of the Hessian matrix with respect to the 8 uncertain parameters have been computed using finite-differences for different values of the step i.e.  $\text{eps} = 10^{-4}, 10^{-5}, 10^{-6}$ , values that are quite reasonable for the case of second-order sensitivity derivatives. The computed Hessian matrix components using finite differences are quite different compared with each other revealing that the Hessian computed using the adjoint approach is very difficult to be validated, as illustrated in Fig. 1.

For both prediction error models, full convergence was obtained after almost 50 optimization cycles. The computational cost for each cycle was equal to approximately 30 s, 15 s for the convergence of the solution of the flow equations and 15 s for the convergence of the corresponding adjoint equations to machine accuracy, at an Intel Core i7 computer at 3.7 GHz. The computation of the Hessian matrix of the second-order sensitivity derivatives of the objective function with respect to the eight Spalart–Allmaras model parameters required also about 15 s for each parameter, almost equal to that of the solution of

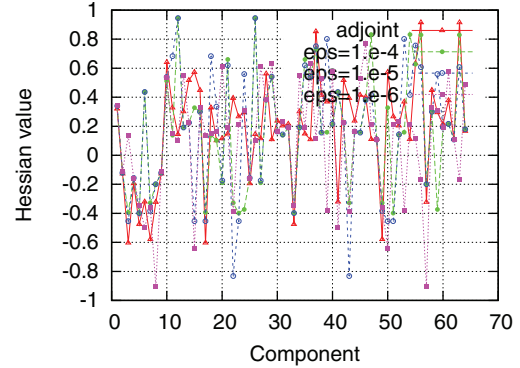


**Fig. 1.** Comparison of the Hessian matrix values computed using the adjoint approach and the finite-differences method for different values of the step.

**Table 2**

Flat plate: Initial and optimal parameter values and coefficients of variation (COV) using the adjoint approach for the correlated and the uncorrelated case (rest four parameters).

	$c_{w_3}$	$\sigma_{SA}$	$\sigma_{\text{VEL}}$	$\lambda_{\text{VEL}}$
Nominal value	2.000	0.667	–	–
Optimal value (correlated)	2.004	0.811	0.167	10.04
Optimal value (uncorrelated)	2.006	0.850	0.154	–
COV (prior)	0.200	0.200	–	–
COV (posterior, correlated)	0.198	0.160	0.042	7.138
COV (posterior, uncorrelated)	0.197	0.151	0.034	–

the flow or adjoint equations. Thus, the total CPU cost for the computation of the Hessian matrix is almost 2 min added to the 30 s of the direct and adjoint solver at the first cycle. The computation of first and second-order sensitivity derivatives of the objective function  $L(\underline{\theta})$  with respect to the prediction error parameters  $\sigma$  and  $\lambda$  has negligible additional computational cost. Also, the flow and adjoint solution at each optimization cycle was initiated from the corresponding solutions at the previous cycle, resulting to a total computational cost of about half an hour for the entire optimization.

In Tables 1 and 2, the initial and optimal values of the parameters using the proposed method are shown for the correlated and uncorrelated prediction error model, respectively. The coefficients of variation (COV) of the updated marginal distribution of each model parameter, defined as the ratio of the standard deviation over the mean (optimal) value of each model parameter, are also reported in these tables. For the Gaussian posterior distribution, the standard deviation of the  $i$ th parameter is the square root of the  $i$  diagonal element of the covariance matrix. The experimental data are informative for a particular turbulence model parameter if the COV of the marginal posterior PDF of this parameter is reduced compared to the COV of the prior PDF. It can be seen from the results in Tables 1 and 2 that the most well-informed parameters are  $\kappa$ ,  $c_{v_1}$  and  $c_{b_1}$ . The results for  $\kappa$  and  $c_{v_1}$  are consistent with the results obtained in [66]. The uncertainty in  $c_{w_2}$  and  $\sigma_{SA}$  has a smaller reduction in relation to the prior uncertainty. The rest of the parameters  $c_{v_2}$ ,  $c_{b_2}$  and  $c_{w_3}$  retained the

**Table 3**Flat plate: Correlation coefficient  $\rho_{ij}(\times 100)$  between the model parameters (correlated error model).

	$\kappa$	$c_{v_1}$	$c_{v_2}$	$c_{b_1}$	$c_{b_2}$	$c_{w_2}$	$c_{w_3}$	$\sigma_{SA}$	$\sigma_{VEL}$	$\lambda_{VEL}$
$\kappa$	100.0	93.0	2.0	-49.0	9.0	-21.0	-2.0	-21.0	8.0	-7.0
$c_{v_1}$	93.0	100.0	2.0	-67.0	7.0	-17.0	-2.0	-12.0	4.0	-6.0
$c_{v_2}$	2.0	2.0	100.0	-2.0	3.0	-2.0	-0.0	-3.0	8.0	5.0
$c_{b_1}$	-49.0	-67.0	-2.0	100.0	-22.0	-15.0	-0.0	-41.0	18.0	10.0
$c_{b_2}$	9.0	7.0	3.0	-22.0	100.0	-3.0	-0.0	-7.0	20.0	11.0
$c_{w_2}$	-21.0	-17.0	-2.0	-15.0	-3.0	100.0	-0.0	3.0	-19.0	-12.0
$c_{w_3}$	-2.0	-2.0	-0.0	-0.0	-0.0	-0.0	100.0	0.0	-1.0	-1.0
$\sigma_{SA}$	-21.0	-12.0	-3.0	-41.0	-7.0	3.0	0.0	100.0	-47.0	-27.0
$\sigma_{VEL}$	8.0	4.0	8.0	18.0	20.0	-19.0	-1.0	-47.0	100.0	59.0
$\lambda_{VEL}$	-7.0	-6.0	5.0	10.0	11.0	-12.0	-1.0	-27.0	59.0	100.0

**Table 4**Flat plate: Correlation coefficient  $\rho_{ij}(\times 100)$  between the model parameters (uncorrelated error model).

	$\kappa$	$c_{v_1}$	$c_{v_2}$	$c_{b_1}$	$c_{b_2}$	$c_{w_2}$	$c_{w_3}$	$\sigma_{SA}$	$\sigma_{VEL}$
$\kappa$	100.0	95.0	4.0	-57.0	15.0	-26.0	-2.0	-27.0	19.0
$c_{v_1}$	95.0	100.0	4.0	-69.0	12.0	-20.0	-2.0	-17.0	13.0
$c_{v_2}$	4.0	4.0	100.0	-3.0	4.0	-2.0	-0.0	-4.0	10.0
$c_{b_1}$	-57.0	-69.0	-3.0	100.0	-28.0	-15.0	-0.0	-38.0	17.0
$c_{b_2}$	15.0	12.0	4.0	-28.0	100.0	-4.0	-0.0	-9.0	22.0
$c_{w_2}$	-26.0	-20.0	-2.0	-15.0	-4.0	100.0	-0.0	4.0	-21.0
$c_{w_3}$	-2.0	-2.0	-0.0	-0.0	-0.0	-0.0	100.0	0.0	-1.0
$\sigma_{SA}$	-27.0	-17.0	-4.0	-38.0	-9.0	4.0	0.0	100.0	-49.0
$\sigma_{VEL}$	19.0	13.0	10.0	17.0	22.0	-21.0	-1.0	-49.0	100.0

COV at approximately the level given by the prior Gaussian distribution, indicating that the data do not provide valuable information for identifying the values and uncertainty in these parameters.

Note that global sensitivity studies using Sobol indices could be alternatively performed to identify the insensitive parameters before the calibration step, as it was done in [13] for similar flow problems. Such sensitivity studies applied for similar problems in [65] can be efficiently performed here using the proposed adjoint formulation. However, the use of Gaussian priors allows one to maintain all parameters in the inference and propagate their uncertainties imposed by the prior to important QoI.

Comparing the optimal values of the model parameters obtained for the uncorrelated and correlated cases a less than 5% difference is observed. For the COV, these differences are less than 10%. Both cases provide consistent results about the values and uncertainties of the turbulence model parameters.

Tables 3 and 4 present results for correlation coefficient between the parameters of the model. Given the covariance matrix  $C \equiv C(\hat{\theta}) = H^{-1}(\hat{\theta})$  of the posterior distribution of the model parameters, the correlation coefficient  $\rho_{ij}$  between the  $i$ th and the  $j$ th parameter is defined as  $\rho_{ij} = C_{ij} / \sqrt{C_{ii}C_{jj}}$  ( $|\rho_{ij}| \leq 1$ ). Strong correlations ( $\rho_{ij} > 0.7$ ) are observed for the two turbulence model parameters ( $\kappa, c_{v_1}$ ). The strong correlation observed is consistent with the correlation between the same parameters presented in [11] using a different method (a stochastic simulation based on MCMC). Moderate correlations ( $0.4 \leq \rho_{ij} \leq 0.7$ ) are obtained for the two turbulence model parameter pairs ( $\kappa, c_{b_1}$ ) and ( $c_{v_1}, c_{b_1}$ ), the model and the prediction error parameter pair ( $\sigma_{SA}, \sigma_{VEL}$ ) and the model prediction error parameter pair ( $\sigma_{VEL}, \lambda_{VEL}$ ). Weaker correlations ( $0.1 \leq \rho_{ij} \leq 0.4$ ) are obtained for 14 parameter pairs, while for the rest 26 parameter pairs the correlation coefficient is less than 0.1. In the spatially uncorrelated model prediction error case, a similar pattern of correlation coefficients arises as it can be seen by comparing the values in Tables 3 and 4.

The uncertainties identified for the model parameters are propagated through the model in order to make robust predictions of output QoI. Two types of output QoI are considered. The first type involves the thirteen axial velocities along the profile for  $y^+ < 400$

that were used for parameter estimation. The second type includes four axial velocities for  $y^+ > 400$  that were not considered in the calibration process. All experimental values are taken from DNS simulations. The mean values and the uncertainties of the 17 axial velocities are compared with the corresponding experimental values in Fig. 2. Two cases are considered. In the first case, only parametric uncertainties identified by the calibration procedure based on the thirteen experimental velocity values are propagated. In the second case, both parametric and model error uncertainties are propagated. The uncertainty region predicted by the model is quantified by the mean plus or minus three standard deviations, where the standard deviations are obtained by considering either the parametric uncertainties or both the parametric and model uncertainties. The experimental values considered in the calibration process are well captured by considering only the parametric uncertainties. This is true not only for the velocities for  $y^+ < 400$ , used for calibration, but also for the velocities for  $y^+ > 400$  that were not taken into account during the inverse quantification process. It is worth noting that the uncertainty in the output QoI that is obtained by propagating only the uncertainty in the turbulence model parameters contains all experimental values. This is an indication that the turbulence model is quite adequate to quantify the flat plate flow for the present flow conditions. The inclusion of the uncertainty due to the prediction error, given by Eq. (13), slightly increases the uncertainty bounds of the output QoI.

The two competing, spatially uncorrelated and correlated prediction error model classes are compared in order to select the best model class given the experimental data. Assuming the same prior probability for each model class, the most appropriate model class is the one with the highest evidence value. The logarithm of the evidence of the correlated prediction error model is equal to 51.90, while that of the uncorrelated model is equal to 50.14. Assuming equal prior probabilities for the correlated and uncorrelated model classes, the relative probabilities are 0.85 and 0.15 for the correlated and uncorrelated model classes, respectively. These probability values promote the correlated model class as more probable, but are not sufficiently different so as to completely disregard the importance of the uncorrelated model class in Bayesian predictions.



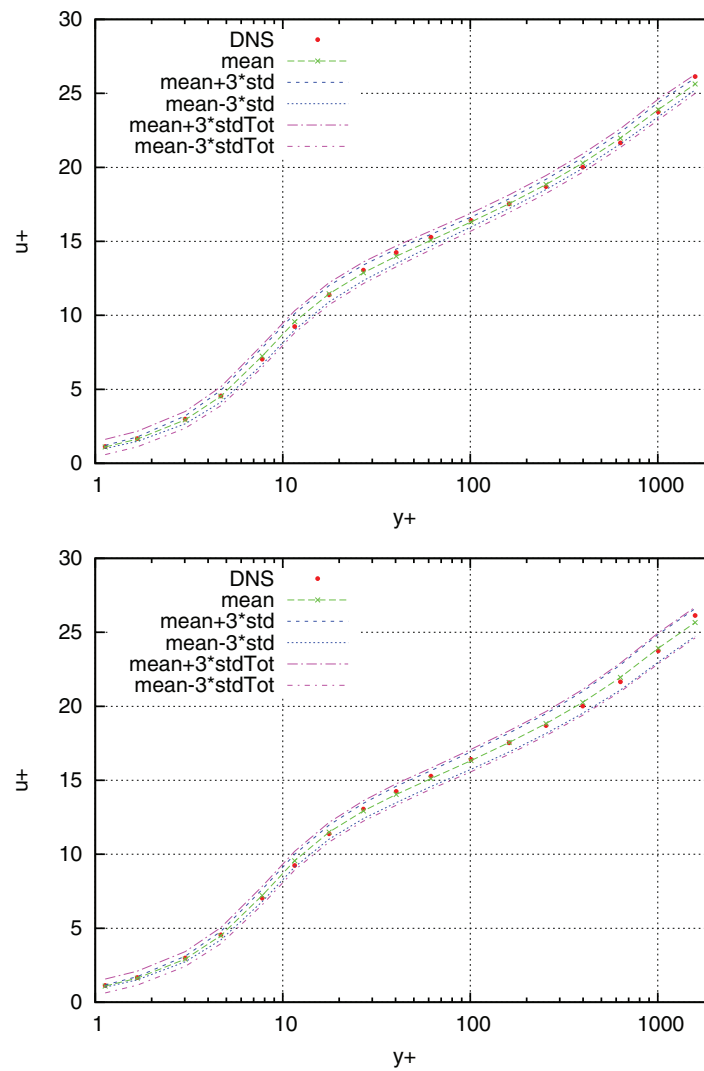


**Fig. 2.** Flat plate: Mean values and spread of uncertainty of the computed velocities at location  $Re_\theta = 6000$  for the optimal values of the parameters, for the correlated and uncorrelated case with the experimental distributions based on DNS. Mean  $\pm 3\text{std}$  is based only on parameter uncertainty, while mean  $\pm 3\text{stdTot}$  is based on both parameter and prediction error uncertainty.

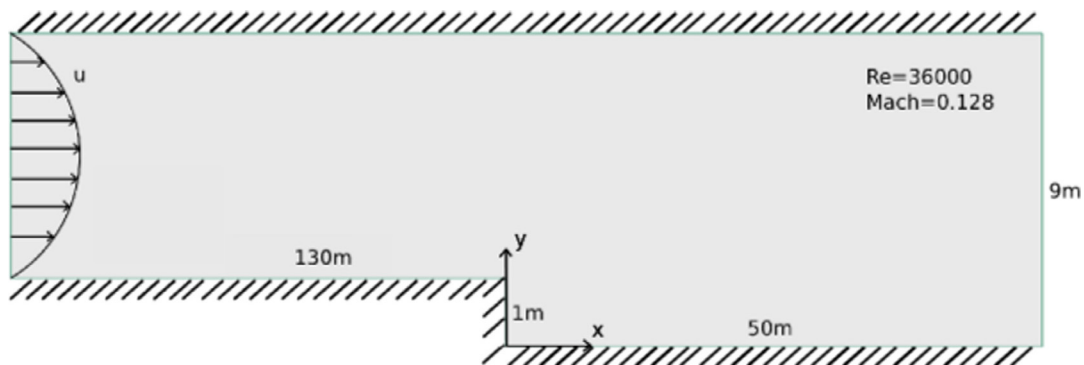


**Fig. 3.** Schematic view of the backward facing step case.

## 6.2. Backward facing step case

The proposed algorithm is also applied to the quantification of the uncertainties of the eight parameters of the Spalart–Allmaras turbulence model and the parameters of the prediction error model in the flow through a 2D backward facing step configuration [69]. The flow

domain is shown in Fig. 3, used in [http://turbmodels.larc.nasa.gov/backstep\\_val.html](http://turbmodels.larc.nasa.gov/backstep_val.html). The turbulent boundary layer encounters a sudden back step, causing flow separation. The flow then reattaches and recovers downstream of the step. The Reynolds number based on step height is equal to 36,000 and the inlet Mach number is equal to 0.128. The step height is equal to 1m, while the distance between the top

**Table 5**

Backward facing step: Initial and optimal parameter values and coefficients of variation (COV) using the adjoint approach for the correlated and the uncorrelated case (first six parameters).

	$\kappa$	$c_{v_1}$	$c_{v_2}$	$c_{b_1}$	$c_{b_2}$	$c_{w_2}$
Nominal value	0.410	7.100	5.000	0.1355	0.622	0.300
Optimal value (correlated)	0.471	6.817	4.950	0.1039	0.639	0.314
Optimal value (uncorrelated)	0.456	7.591	4.749	0.1102	0.637	0.335
COV (prior)	0.200	0.200	0.200	0.2000	0.200	0.200
COV (posterior, correlated)	0.109	0.126	0.195	0.0712	0.193	0.172
COV (posterior, uncorrelated)	0.087	0.097	0.200	0.0535	0.194	0.175

**Table 6**

Backward facing step: Initial and optimal parameter values and coefficients of variation (COV) using the adjoint approach for the correlated and the uncorrelated case (rest six parameters).

	$c_{w_3}$	$\sigma_{SA}$	$\sigma_{VEL}$	$\lambda_{VEL}$	$\sigma_{RS}$	$\lambda_{RS}$
Nominal value	2.000	0.667	0.035	0.800	1.000	0.200
Optimal value (correlated)	1.976	0.770	0.036	0.819	1.156	0.248
Optimal value (uncorrelated)	2.074	0.915	0.039	–	1.436	–
COV (prior)	0.200	0.200	–	–	–	–
COV (posterior, correlated)	0.200	0.148	0.145	0.386	0.073	0.189
COV (posterior, uncorrelated)	0.178	0.120	0.062	–	0.064	–

**Table 7**

Backward facing step: Correlation coefficient  $\rho_{ij}$  (x100) between the model parameters (correlated error model).

	$\kappa$	$c_{v_1}$	$c_{v_2}$	$c_{b_1}$	$c_{b_2}$	$c_{w_2}$	$c_{w_3}$	$\sigma_{SA}$	$\sigma_{VEL}$	$\lambda_{VEL}$	$\sigma_{RS}$	$\lambda_{RS}$
$\kappa$	100	71	–5	–44	4	–1	3	8	–5	3	–1	–18
$c_{v_1}$	71	100	–18	–1	1	8	3	26	–30	–25	–9	–32
$c_{v_2}$	–5	–18	100	8	0	4	1	11	–8	–9	–1	–2
$c_{b_1}$	–44	–1	8	100	–18	–9	4	–44	–20	–19	5	–16
$c_{b_2}$	4	1	0	–18	100	1	–0	–1	–2	–1	–1	–1
$c_{w_2}$	–1	8	4	–9	1	100	–1	–6	1	3	–0	–1
$c_{w_3}$	3	3	1	4	–0	–1	100	–3	–2	–2	2	1
$\sigma_{SA}$	8	26	11	–44	–1	–6	–3	100	9	9	–15	–8
$\sigma_{VEL}$	–5	–30	–8	–20	–2	1	–2	9	100	90	4	8
$\lambda_{VEL}$	3	–25	–9	–19	–1	3	–2	9	90	100	5	5
$\sigma_{RS}$	–1	–9	–1	5	–1	–0	2	–15	4	5	100	48
$\lambda_{RS}$	–18	–32	–2	–16	–1	–1	1	–8	8	5	48	100

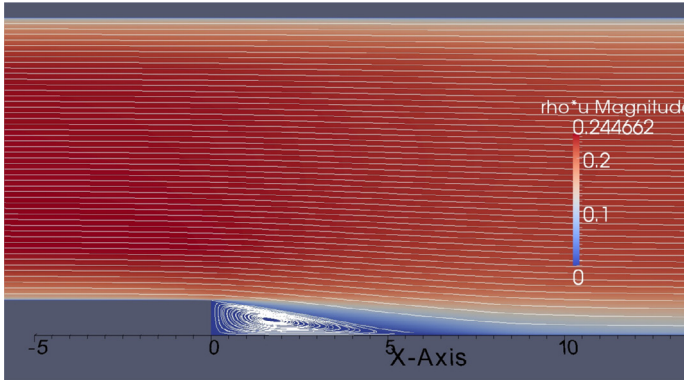


**Fig. 4.** Velocity streamlines and contours corresponding to the initial set of parameters.

and bottom walls is equal to 9m (after the step). The velocity streamlines within the flow domain are illustrated in Fig. 4 for the nominal value of the parameter set  $\underline{\theta}$ .

The experimental data used for the quantification of uncertainties are the axial velocity and Reynolds shear stress profiles at five longitudinal positions. The experimental data and the measured positions within the flow domain can be found in [69] and in the aforementioned site of NASA. The first position is 4m before the step and the other four ones are 1m, 4m, 6m and 10m after the step. A computa-

tional grid with 4992 quadrilateral elements, obtained from the same site, is used to carry out the simulations.

Similar to the flat plate test case Gaussian prior distribution of the parameters are assumed for the turbulent model parameters and uniform for the prediction error parameters. The uncertainty domains are selected the same as in the flat plate test case.

Here the error term  $\underline{e} = (\underline{e}_{VEL}, \underline{e}_{RS})$  is partitioned into two vectors, with  $\underline{e}_{VEL}$  and  $\underline{e}_{RS}$  associated with the velocity and Reynolds stress measurements, respectively. The error terms for the velocity and the Reynolds stresses are assumed to be independent. This yields a block partitioned diagonal covariance matrix  $\Sigma = \text{diag}(\Sigma_{VEL}, \Sigma_{RS})$ . Two prediction error models are considered. The first prediction error model assumes spatially uncorrelated errors with the covariance matrix for the velocity and Reynolds stress prediction errors represented in the form  $\Sigma = \text{diag}(\sigma_{VEL}^2 I_{VEL}, \sigma_{RS}^2 I_{RS})$ , where  $I_{VEL}$  and  $I_{RS}$  are identity matrices and  $\sigma_{VEL}$  and  $\sigma_{RS}$  are the constant standard deviations assumed for velocity and Reynold stress measurements, respectively. The parameter set  $\underline{\theta}^e$  associated with the uncorrelated prediction error model is  $\underline{\theta}^e = (\sigma_{VEL}, \sigma_{RS})$ . The second prediction error model that assumes that the errors between two measurement locations are spatially correlated. The diagonal block elements in  $\Sigma$  are full matrices which depend on the spatial correlation structure assumed for the model errors. The exponential correlation structure given by Eq. (47) is assumed for the components ( $k, l$ ) of the diagonal block matrices  $\Sigma_{VEL}$  and  $\Sigma_{RS}$ , where the subscript  $a$  in Eq. (47) stands for either VEL or RS. In this case the parameter set  $\underline{\theta}^e$  associated with the correlated prediction error model is  $\underline{\theta}^e = (\sigma_{VEL}, \lambda_{VEL}, \sigma_{RS}, \lambda_{RS})$ .

**Table 8**

Backward facing step: Correlation coefficient  $\rho_{ij}(\times 100)$  between the model parameters (uncorrelated error model).

	$\kappa$	$c_{\nu_1}$	$c_{\nu_2}$	$c_{b_1}$	$c_{b_2}$	$c_{w_2}$	$c_{w_3}$	$\sigma_{SA}$	$\sigma_{VEL}$	$\sigma_{RS}$
$\kappa$	100	81	-6	-58	6	-1	-4	3	2	-10
$c_{\nu_1}$	81	100	-22	-29	-2	10	1	28	6	-18
$c_{\nu_2}$	-6	-22	100	7	1	5	0	8	1	1
$c_{b_1}$	-58	-29	7	100	-30	-13	12	-31	2	10
$c_{b_2}$	6	-2	1	-30	100	0	-3	-2	-1	-0
$c_{w_2}$	-1	10	5	-13	0	100	2	-5	-4	-3
$c_{w_3}$	-4	1	0	12	-3	2	100	2	-3	1
$\sigma_{SA}$	3	28	8	-31	-2	-5	2	100	1	-21
$\sigma_{VEL}$	2	6	1	2	-1	-4	-3	1	100	-2
$\sigma_{RS}$	-10	-18	1	10	-0	-3	1	-21	-2	100

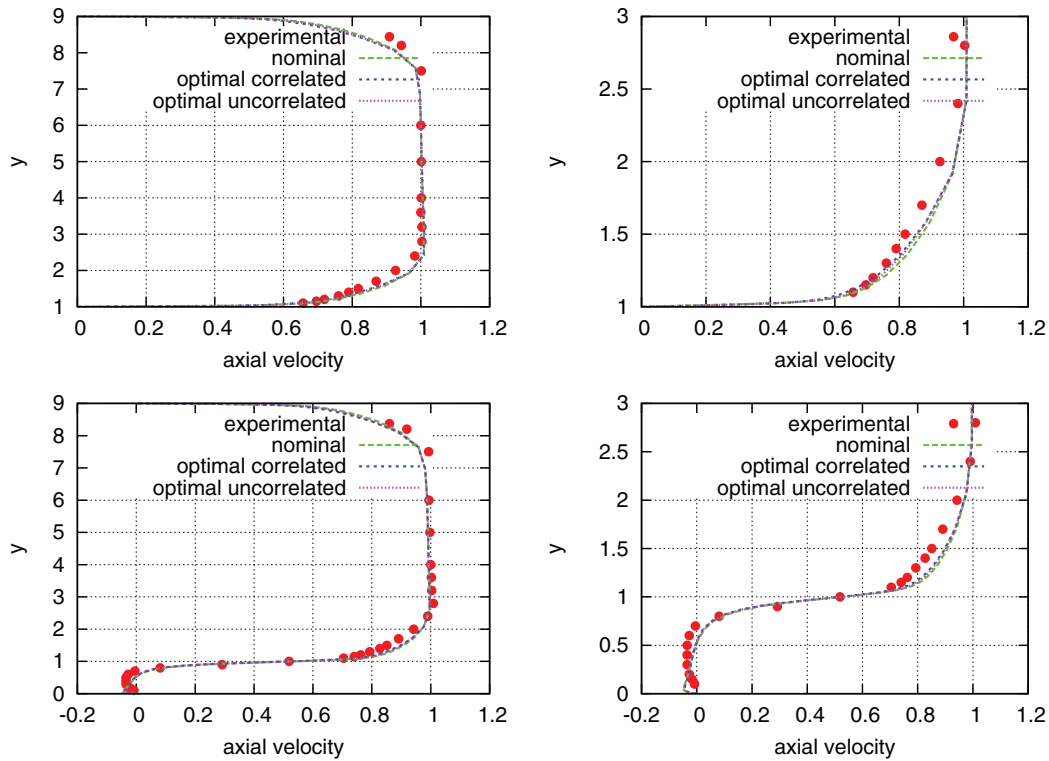


**Fig. 5.** Comparison of the optimal velocity distributions at location 4m before (top) and 1m after (bottom) before the step based on the optimal values of the model parameters for the correlated and uncorrelated case with the experimental distributions based on measurements. The right figures are close-up views at the separation region where  $y < 3$ .

For both prediction error models, full convergence was obtained after almost 40 optimization cycles. The computational cost for each cycle was equal to approximately 4 min, 2 min for the flow equations and 2 min for the adjoint equations. The computation of the Hessian matrix with respect to the eight Spalart–Allmaras model parameters required also about 2 min for each parameter, almost equal to that of the solution of the flow or adjoint equations. Thus, the total CPU cost is almost one and a half hour for the entire optimization.

In Tables 5 and 6, the initial and optimal values of the parameters using the proposed method are shown for the correlated and uncorrelated prediction error model, respectively, along with the COV of the marginal distribution of each model parameter. The results are qualitatively similar to those obtained in the previous test case of the flow above the flat plate. Specifically, as in the flat plate problem, the most well-informed parameters are  $\kappa$ ,  $c_{\nu_1}$  and  $c_{b_1}$ . The parameters  $c_{w_2}$  and  $\sigma_{SA}$  are also informed with a small reduction in uncertainty in relation to the prior uncertainty, while the remaining three parameters  $c_{\nu_2}$ ,  $c_{b_2}$  and  $c_{w_3}$  retain the COV at approximately the level given by the prior Gaussian distribution.

Tables 7 and 8 present results for correlation coefficient between the parameters of the model, resulting also to similar conclusions as in the flat plate case. Specifically, the strongest correlation ( $\rho_{ij} > 0.7$ ) is observed for the two turbulence model parameters ( $\kappa$ ,  $c_{\nu_1}$ ) and moderate correlations ( $0.4 \leq \rho_{ij} \leq 0.7$ ) are obtained for the parameter pairs ( $\kappa$ ,  $c_{b_1}$ ), ( $c_{\nu_1}$ ,  $c_{b_1}$ ), ( $\sigma_{SA}$ ,  $\sigma_{VEL}$ ) and ( $\sigma_{VEL}$ ,  $\lambda_{VEL}$ ). Thus, qualitatively the results of parameter estimation are consistent for both test cases.

The velocity and the Reynolds stress profiles are next computed at the most probable values of the model parameters. The optimal velocity profiles at the five longitudinal positions are compared with the corresponding experimental profiles in Figs. 5 and 6. The left part of the figures show the overall profiles from the bottom surface to the top surface whereas the right parts show the close-up view of the profiles at the separation region ( $y < 3$ ). In almost all of the five plots, it can be seen that the optimal velocity profiles using the correlated and the uncorrelated models are both quite close with each other and also close to the initial ones that correspond to the nominal model parameters. Also, discrepancies are observed between optimal profiles

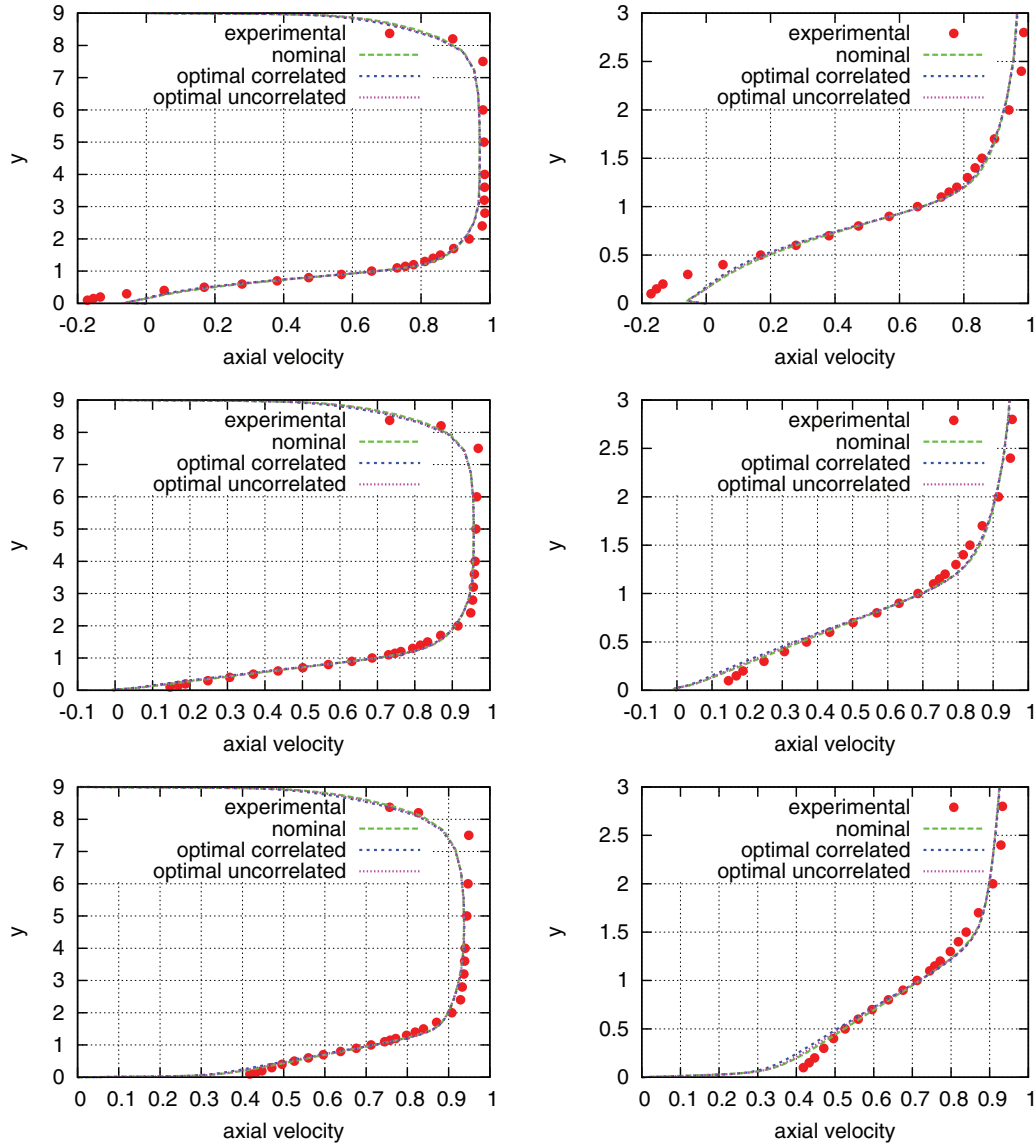


**Fig. 6.** Comparison of the optimal velocity distributions at location 4m (top), 6m (middle) and 10m (bottom) after the step based on the optimal values of the model parameters for the correlated and uncorrelated case with the experimental distributions based on measurements. The right figures are close-up views at the separation region where  $y < 3$ .

and the experimental velocity profiles at locations close to the wall ( $y < 0.5$ ). The discrepancies of the optimal profiles with the experimental ones are quite large for both optimal solutions. All these facts reveal that the velocity predictions are not so sensitive to the values of the Spalart–Allmaras model parameters.

The corresponding Reynolds stress profiles at the same positions are illustrated in Figs. 7 and 8. Here the optimal parameters provide optimal profiles that are different from the nominal ones which means that the Reynolds stress profiles are more sensitive to the values of the Spalart–Allmaras parameters. This is expected, since the Reynolds stresses are directly expressed in terms of the turbulence model parameters through the turbulence viscosity. Also, it can be seen that, similar to the case of the velocity profiles, there are discrepancies between the optimal curves and the experimental ones indicating that the Spalart–Allmaras model is not so adequate for such computations, where massive separation takes place, even if the model parameters are optimally identified.

The identified uncertainties in the turbulence model parameters and the prediction error model parameters are propagated through

the model to evaluate the uncertainties in important QoI. First, velocities and Reynolds stresses are considered for which experimental measurements are available. The propagation of the uncertainties in the velocity and Reynolds stresses at three selected locations for each output quantity are shown in Table 9 for the case of the spatially correlated prediction error model. The six points were chosen such that the deviation of the computed quantities from the experimental ones is relatively high. The results in Table 9 include established indices that quantify uncertainty in a variable  $g(\theta, \eta)$ , such as mean, optimal value, standard deviation  $STD(g_m(\theta))$ , derived from (14), measuring the uncertainty due to the uncertainty in the turbulence model parameters, standard deviation  $\sigma_\eta$  of the prediction error given in (10) and the overall standard deviation in (12) that combines parameter and prediction error uncertainties in evaluating the uncertainty in the output QoI. The experimental values of the velocities and Reynolds stresses are also included in Table 9 and Figs. 5–8, for comparison purposes.

It can be observed that, in all these cases, the standard deviation  $\sigma_{VEL}$  and  $\sigma_{RS}$  of the prediction error model is significantly higher than



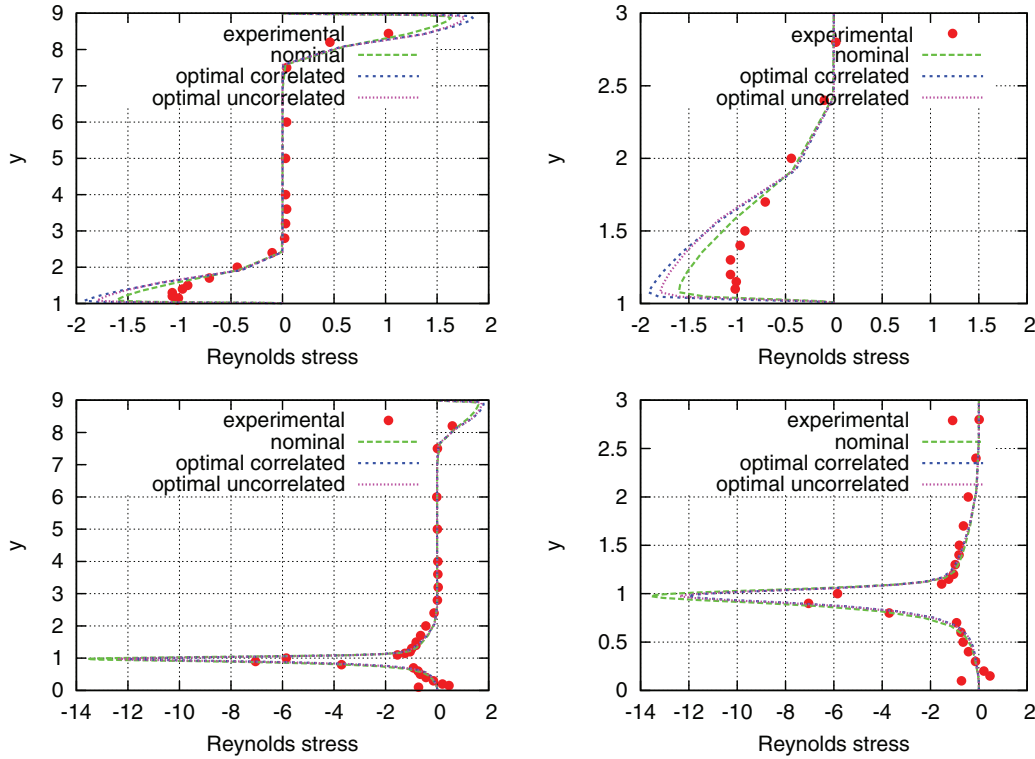


**Fig. 7.** Comparison of the optimal Reynolds stress distributions at location 4m before (top) and 1m after (bottom) the step based on the optimal values of the model parameters for the correlated and uncorrelated case with the experimental distributions based on measurements. The right figures are close-up views at the separation region where  $y < 3$ .

**Table 9**

Backward facing step: Mean, optimal and standard deviations (std) of the velocities and Reynolds stresses at three selected locations (correlated error model).

	$u^{(1)}$	$u^{(2)}$	$u^{(3)}$	$t_{xy}^{(1)}$	$t_{xy}^{(2)}$	$t_{xy}^{(3)}$
$x$	1.0	4.0	6.0	4.0	6.0	10.0
$y$	0.5	0.15	0.15	0.4	0.4	0.6
Experimental value	-0.0350	-0.1540	-0.1690	-12.02	-8.23	-4.61
Optimal value	-0.0043	-0.0075	-0.0980	-4.617	-5.923	-3.43
Mean value	-0.0043	-0.0091	-0.0977	-4.575	-5.872	-3.54
Std $STD[g_m(\theta)]$	0.0008	0.0044	0.0071	0.325	0.250	0.0829
Std $\sigma_{VEL}$ or $\sigma_{RS}$	0.0359	0.0359	0.0359	1.156	1.156	1.156
Total std	0.0359	0.0361	0.0366	1.201	1.183	1.159

the standard deviation  $STD(g_m(\theta))$  computed by propagating only the turbulence model parameter uncertainty. Thus the prediction error uncertainty for these QoI dominates the uncertainty due to the turbulence model parameters. Moreover, the experimental values of the QoI fall, in most cases, within the uncertainty interval  $[E[g_m(\theta)] - \alpha STD(g_m(\theta)), E[g_m(\theta)] + \alpha STD(g_m(\theta))]$  ( $\alpha \approx 2$  or  $3$ ) predicted for the corresponding QoI, validating the whole uncertainty quantification methodology. However, the experimental values fall outside the uncertainty interval  $[E[g_m(\theta)] - \alpha STD(g_m(\theta)), E[g_m(\theta)] + \alpha STD(g_m(\theta))]$  computed based only on the uncertainty of the turbulence model parameters, ignoring the prediction error model uncertainty. This discrepancy is also an indication that the selected turbulent model does not predict well the experimental data and a more suitable turbulence model should be used. Finding the best turbulence model, however, is not the objective of this study which concentrates on integrating Bayesian analytical approximations with higher-order adjoint techniques for quantifying uncertainties in turbulence modeling within CFD. Apart from the fact that the Spalart–Allmaras turbulence model is proved to be inappropriate for the prediction of the backward-facing step flow, an important source of difference is due to the experimental limitations since, for instance, the flow profile at the step inlet is not fully developed. This may have a substantial

effect on the downstream flow which could even dominate the effect of turbulence modeling.

Next, the Bayesian asymptotic analysis is used to propagate uncertainties to the total pressure losses, computed as the difference in average total pressure  $p_t$  between the inlet and the outlet of the flow domain  $A_I^{-1} \int_{S_I} p_t dS - A_O^{-1} \int_{S_O} p_t dS$ , where  $A_I$  and  $A_O$  are the inlet and outlet areas, respectively. Accounting for the uncertainty in the turbulence model parameters, the predicted mean value is equal to  $2.752E-3$  and the standard deviation is equal to  $1.250E-4$ , which corresponds to coefficient of variation of 4.5%, for the correlated model error case. In the case of the uncorrelated error model the mean value of the total pressure losses is equal to  $2.277E-3$  and the standard deviation is equal to  $1.592E-4$ , which corresponds to coefficient of variation of 6.7%. It seems that the uncertainty propagation results depend on the prediction error model used. Finally, it should be noted that the uncertainties reported ignore uncertainties due to prediction error model that arise from the model inadequacy. In contrast to the velocity and Reynolds stresses, there is no information to compute such prediction error uncertainties since the experimental values of the pressure losses are not available. As it was derived in the theory (see Eq. (14)), the prediction error model uncertainties will be insignificant for standard deviations  $\sigma_\eta$  much smaller than

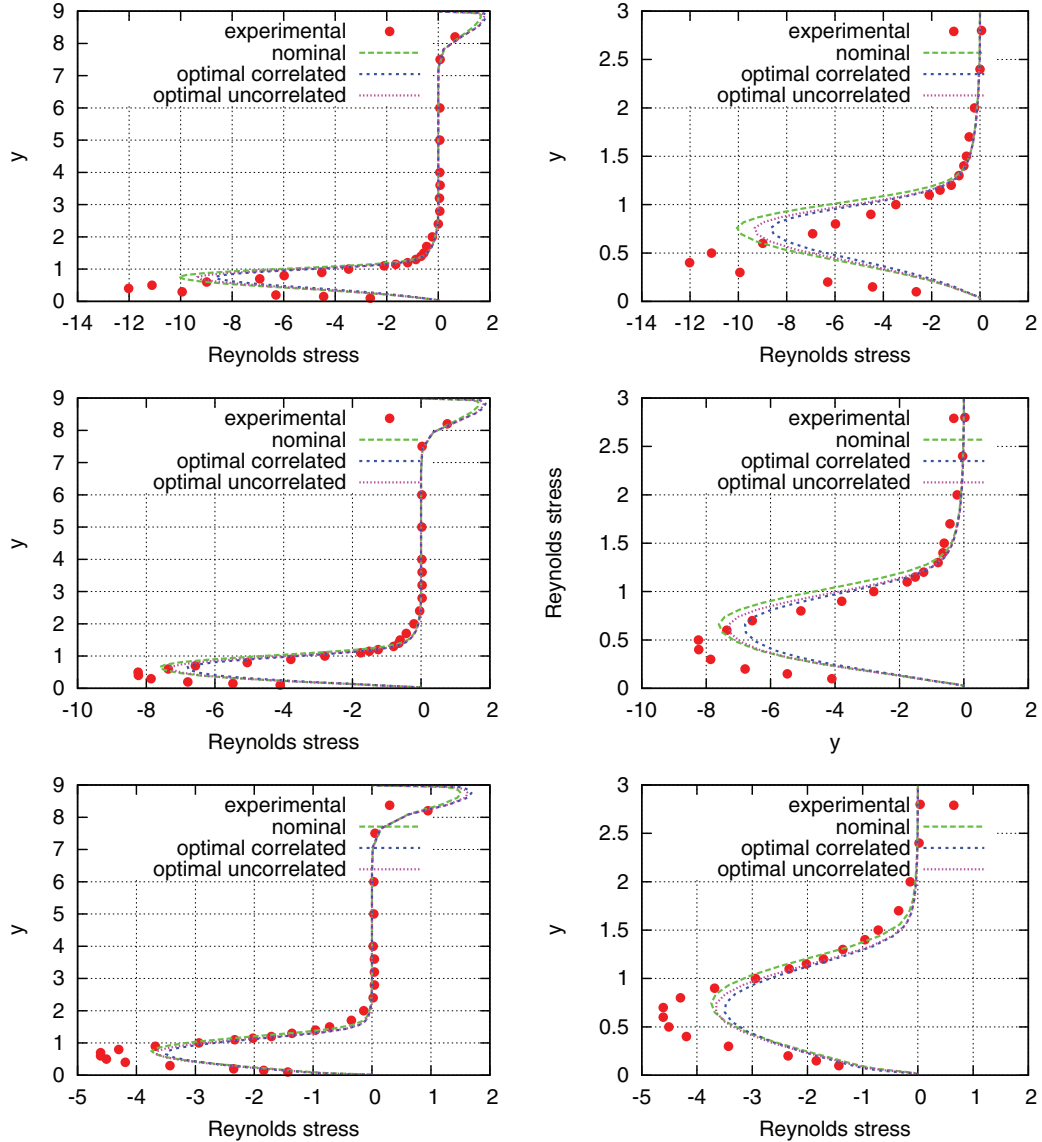


**Fig. 8.** Comparison of the optimal Reynolds stress distributions at location 4m (top), 6m (middle) and 10m (bottom) after the step based on the optimal values of the model parameters for the correlated and uncorrelated case with the experimental distributions based on measurements. The right figures are close-up views at the separation region where  $y < 3$ .

the standard deviations  $\text{STD}(g_m(\theta))$  derived from the uncertainties in the model parameters. However, for standard deviations  $\sigma_\eta$  much larger than the ones derived from the uncertainties in the model parameters, the prediction error uncertainties will dominate the overall uncertainty in the pressure losses.

Finally, the two competing, spatially uncorrelated and correlated prediction error model classes are compared in order to select the best model class given the experimental data. The logarithm of the evidence of the correlated prediction error model is equal to 251.34, while that of the uncorrelated model is equal to 117.41. The most important term that made this difference was the second term of Eq. (30) that depends directly on the determinant of the covariance matrix  $\Sigma$ ; the other terms were quite similar for the two models which was expected since the optimal profiles found using the two models were quite alike. The large differences in the values of the logarithm of the evidences indicate that the correlation between the errors is quite important and that the spatially correlated prediction error model is the best model among the two, justifying that the spatial correlation should be taken into account in modeling prediction errors in this flow problem.

## 7. Conclusions

A Bayesian framework was presented for uncertainty quantification and propagation in turbulence models employed in CFD simulations. Bayesian techniques combining analytical asymptotic approximations with higher-order adjoint methods developed for CFD simulations were used to estimate the posterior PDF of the flow and prediction error model parameters, select the best model among competitive prediction error models and propagate uncertainties through CFD model simulations for making robust predictions of important output QoI. The adjoint formulation requires a relatively small number of forward and adjoint system re-analyses in relation to the very large number of system re-analyses required in computationally very demanding stochastic simulation algorithms. This computational efficiency, however, comes with the extra burden of developing the adjoint formulations and integrating them in system simulation software, a procedure that can be quite cumbersome for a number of turbulence models employed in CFD simulations.

The proposed framework was applied for the estimation of the parameters of the Spalart–Allmaras turbulence model based on

velocity “measurements” at a flat plate flow, and velocity and Reynolds stress measurements at a backward facing step flow. Results clearly demonstrated that the measurements provide information for estimating five among the eight parameters of the turbulence model, while the rest of the parameters were insensitive to the information contained in the data. Model validation using the experimental measurements suggest that the Spalart–Allmaras model is quite adequate to accurately predict velocities in the flat plate flow case. However, it was found inadequate to accurately predict velocities and Reynolds stresses in certain region in the flow domain of the backward facing step flow, where flow separation phenomena are dominant. The inadequacy is manifested by the high prediction error uncertainty in these regions in relation to the prediction uncertainty arising from the turbulence model parameter uncertainty. Among the two prediction error model classes considered, the spatially correlated one was promoted as the best model by the Bayesian model selection methodology, confirming recent results stating the importance of including spatial correlation in prediction error models.

## Acknowledgments

The research project is implemented within the framework of the Action “Supporting Postdoctoral Researchers” of the Operational Program “Education and Lifelong Learning” (Action’s Beneficiary: General Secretariat for Research and Technology), and is co-financed by the European Social Fund (ESF) and the Greek State.

## References

- Beck JL. Bayesian system identification based on probability logic. *Struct Control Health Monit* 2010;17(7):825–47.
- Yuen KV. Bayesian methods for structural dynamics and civil engineering. John Wiley & Sons; 2010.
- Papadimitriou C, Katafygiotis LS. A Bayesian methodology for structural integrity and reliability assessment. *Int J Adv Manuf Syst* 2001;4(1):93–100.
- Soize C. A computational inverse method for identification of non-Gaussian random fields using the Bayesian approach in very high dimension. *Comput Methods Appl Mech Eng* 2011;200(45–46):3083–99.
- Beck JL, Katafygiotis LS. Updating models and their uncertainties. I: Bayesian statistical framework. *J Eng Mech, ASCE* 1998;124(4):455–61.
- Angelikopoulos P, Papadimitriou C, Koumoutsakos P. Bayesian uncertainty quantification and propagation in molecular dynamics simulations: a high performance computing framework. *J Chem Phys* 2012;137(14):103–44.
- Wang J, Zabaras N. A Bayesian inference approach to the inverse heat conduction problem. *Int J Heat Mass Transf* 2004;47:3927–41.
- Constantine PG, Doostan A, Wang Q, Iaccarino G. A surrogate accelerated Bayesian inverse analysis of the HyShot II flight data. *AIAA paper* 2011–2037 2011.
- Jategaonkar R, Fischenberg D, Gruenhagen W. Aerodynamic modeling and system identification from flight data—recent applications at DLR. *J Aircraft* 2004;41(4).
- Oden JT, Hawkins A, Prudhomme S. General diffuse interface theories and an approach to predictive tumor growth modeling. *Math Models Methods Appl Sci* 2010;20(3):477–517.
- Cheung SH, Oliver TA, Prudencio EE, Prudhomme S, Moser RD. Bayesian uncertainty analysis with applications to turbulence modeling. *Reliab Eng Syst Saf* 2011;96:1137–49.
- Oliver TA, Moser RD. Bayesian uncertainty quantification applied to RANS turbulence models. *J Phys Conf Ser* 2011;318. doi:10.1088/1742-6596/318/4/042032.
- Edeling WN, Cinnella P, Dwight RP, Bijl H. Bayesian estimates of parameter variability in the  $k$ - $\epsilon$  turbulence model. *J Comput Phys* 2014;258:73–94.
- Arnst M, Ghanem R, Soize C. Identification of Bayesian posteriors for coefficients of chaos expansions. *J Comput Phys* 2010;229(9):3134–54.
- Papadimitriou C, Beck JL, Katafygiotis LS. Updating robust reliability using structural test data. *Probab Eng Mech* 2001;16(2):103–13.
- Beck JL, Yuen KV. Model selection using response measurements: Bayesian probabilistic approach. *J Eng Mech, ASCE* 2004;130(2):192–203.
- Cheung SH, Beck JL. Calculation of posterior probabilities for Bayesian model class assessment and averaging from posterior samples based on dynamic system data. *J Comput-Aided Civil Infrastruct Eng* 2010;25(5):304–21.
- Papadimitriou C, Katafygiotis LS. Bayesian modeling and updating. In: Nikolaidis N, Ghiocel DM, Singhal S, editors. *Engineering design reliability handbook*. CRC Press; 2004.
- Tierney L, Kadane JB. Accurate approximations for posterior moments and marginal densities. *J Am Stat Assoc* 1986;81(393):82–6.
- Metropolis N, Rosenbluth AW, Rosenbluth MN, Teller AH, Teller E. Equation of state calculations by fast computing machines. *J Chem Phys* 1953;21(6):1087–92.
- Beck JL, Au SK. Bayesian updating of structural models and reliability using Markov chain Monte Carlo simulation. *ASCE J Eng Mech* 2002;128(4):380–91.
- Ching J, Chen YC. Transitional Markov chain Monte Carlo method for Bayesian updating, model class selection, and model averaging. *J Eng Mech, ASCE* 2007;133:816–32.
- Haario H, Laine M, Mira A, Saksman E. DRAM: efficient adaptive MCMC. *Stat Comput* 2006;16:339–54.
- Cheung SH, Beck JL. Bayesian model updating using hybrid Monte Carlo simulation with application to structural dynamic models with many uncertain parameters. *J Eng Mech, ASCE* 2009;135(4):243–55.
- Margheri L, Meldi M, Salvetti MV, Sagaut P. Epistemic uncertainties in RANS model free coefficients. *Comput Fluids* 2014;102:315–35.
- Angelikopoulos P, Papadimitriou C, Koumoutsakos P. X-TMCMC: adaptive Kriging for Bayesian inverse modeling. *Comput Methods Appl Mech Eng* 2015;289:409–28.
- Lions JL. *Optimal control of systems governed by partial differential equations*. New York: Springer-Verlag; 1971.
- Pironneau O. On optimum design in fluid mechanics. *J Fluid Mech* 1974;64:97–110.
- Pironneau O. *Optimal shape design for elliptic systems*. New York: Springer-Verlag; 1984.
- Jameson A. Aerodynamic design via control theory. *J Sci Comput* 1988;3:233–60.
- Jameson A, Reuther J. Control theory based airfoil design using the Euler equations. *AIAA paper* 94–4272 1994.
- Jameson A. Optimum aerodynamic design using CFD and control theory. *AIAA paper* 95–1729 1995.
- Jameson A, Pierce N, Martinelli L. Optimum aerodynamic design using the Navier–Stokes equations. *Theor Comput Fluid Dyn* 1998;10:213–37.
- Burgreen GW, Baysal O. Three-dimensional aerodynamic shape optimization using discrete sensitivity analysis. *AIAA J* 1996;34(9):1761–70.
- Anderson WK, Venkatakrishnan V. Aerodynamic design optimization on unstructured grids with a continuous adjoint formulation. *AIAA paper* 97–0643 1997.
- Duta MC, Giles MB, Campobasso MS. The harmonic adjoint approach to unsteady turbomachinery design. *Int J Numer Methods Fluids* 2002;40(3–4):323–32.
- Hazra S, Schulz V, Brezillon J, Gauger N. Aerodynamic shape optimization using simultaneous pseudo-timestepping. *J Comput Phys* 2005;204(1):46–64.
- Papadimitriou DI, Giannakoglou KC. A continuous adjoint method with objective function derivatives based on boundary integrals for inviscid and viscous flows. *Comput Fluids* 2007;36:325–41.
- Sherman LL, Taylor AC III, Green LL, Newman PA, Hou JW, Korivi VM. First- and second-order aerodynamic sensitivity derivatives via automatic differentiation with incremental iterative methods. *J Comput Phys* 1996;129:307–31.
- Papadimitriou DI, Giannakoglou KC. Direct, adjoint and mixed approaches for the computation of Hessian in airfoil design problems. *Int J Numer Methods Fluids* 2008;56:1929–43.
- Zervogiannis T, Papadimitriou DI, Giannakoglou KC. Total pressure losses minimization in turbomachinery cascades using the exact Hessian. *J Comput Methods Appl Mech Eng* 2010;199:2697–708.
- Papadimitriou DI, Giannakoglou KC. Computation of the Hessian matrix in aerodynamic inverse design using continuous adjoint formulations. *Comput Fluids* 2008;37:1029–39.
- Papadimitriou DI, Giannakoglou KC. Aerodynamic shape optimization using first and second order adjoint and direct approaches. *Archiv Comput Methods Eng, (State Art Rev)* 2008;15(4):447–88.
- Papadimitriou DI, Giannakoglou KC. The continuous direct-adjoint approach for second order sensitivities in viscous aerodynamic inverse design problems. *Comput Fluids* 2009;38:1539–48.
- Papadimitriou DI, Giannakoglou KC. Robust design in aerodynamics using third-order sensitivity analysis based on discrete adjoint. Application to quasi-1D flows. *Int J Numer Methods Fluids* 2012;69:691–709.
- Papadimitriou DI, Giannakoglou KC. Third-order sensitivity analysis for robust aerodynamic design using continuous adjoint. *Int J Numer Methods Fluids* 2013;71(5):652–70.
- Tortorelli D, Michaleris P. Design sensitivity analysis: overview and review. *Inverse Probl Eng* 1994;1:71–105.
- Hou GW, Sheen J. Numerical methods for second-order shape sensitivity analysis with applications to heat conduction problems. *Int J Numer Methods Eng* 1993;36:417–35.
- Dimet FXL, Navon IM, Daescu DN. Second-order information in data assimilation. *Mon Weather Rev* 2002;130(3):629–48.
- Turgeon E, Pelletier D, Borggaard J, Etienne S. Application of a sensitivity equation method to the  $k$ - $\epsilon$  model of turbulence. *Optimiz Eng* 2007;8:341–72.
- Caro R, Hay A, Etienne S, Pelletier D. Application of a shape sensitivity equation method to turbulent flow over obstacles. *AIAA paper* 2007–4207 2007.
- Colin E, Etienne S, Pelletier D, Borggaard J. Application of a sensitivity equation method to turbulent flows with heat transfer. *Int J Thermal Sci* 2005;44:1024–38.
- Lee BJ, Kim C. Automated design methodology of turbulent internal flow using discrete adjoint formulation. *Aerospace Sci Technol* 2007;11:163–73.
- Zymaris AS, Papadimitriou DI, Giannakoglou KC, Othmer C. Continuous adjoint approach to the Spalart–Allmaras turbulence model for incompressible flows. *Comput Fluids* 2009;38:1528–38.
- Zymaris AS, Papadimitriou DI, Giannakoglou KC, Othmer C. Adjoint wall functions: A new concept for use in aerodynamic shape optimization. *J Comput Phys* 2010;229:5228–45.
- Emory M, Pecnik R, Iaccarino G. Modeling structural uncertainties in Reynolds-averaged computations of shock/boundary layer interactions. *AIAA paper* 2011–479 2011.

- [57] Dow E, Wang Q. Quantification of structural uncertainties in the *k-omega* turbulence model. AIAA paper 2011-1762 2011.
- [58] Kennedy MC, O'Hagan A. Bayesian calibration of computer models. *J R Stat Soc Ser B (Stat Methodol)* 2001;63(3):425–64.
- [59] Peter JEV, Dwight RP. Numerical sensitivity analysis for aerodynamic optimization: A survey of approaches and applications. *Comput Fluids* 2010;39(3):373–91.
- [60] Bui-Thanh T, Ghattas O, Higdon D. Adaptive Hessian-based non-stationary Gaussian process response surface method for probability density approximation with application to Bayesian solution of large-Scale inverse problems. ICES REPORT 11-32 2011.
- [61] Merle X, Cinnella P. Bayesian quantification of thermodynamic uncertainties in dense gas flows. *Reliab Eng Syst Saf* 2015;134:305–23.
- [62] Papadimitriou C, Beck JL, Katafygiotis LS. Asymptotic expansions for reliability and moments of uncertain systems. *Journal of Engineering Mechanics, ASCE* 1997;123(12):1219–29.
- [63] Spalart P, Allmaras S. A one-equation turbulence model for aerodynamic flows. AIAA paper, 92-0439 1992.
- [64] Ghate DP, Giles MB. Efficient hessian calculation using automatic differentiation. In: 25th AIAA applied aerodynamics conference; 2007. Miami, FL
- [65] Pini M, Cinnella P. Hybrid adjoint-based robust optimization approach for fluid-dynamics problems, AIAA paper 2013-1814. In: 15th non-deterministic approaches conference; 2013. Boston, MA
- [66] Edeling WN, Cinnella P, Dwight RP. Predictive RANS simulations via Bayesian model-scenario averaging. *J Comput Phys* 2014;275:65–91.
- [67] Simens MP, Jimenez J, Hoyas S, Mizuno Y. A high-resolution code for turbulent boundary layers. *J Comput Phys* 2009;228(11):4218–31.
- [68] Borrell G, Sillero JA, Jimenez J. A code for direct numerical simulation of turbulent boundary layers at high Reynolds numbers in BG/P supercomputers. *Comput Fluids* 2013;80:37–43.
- [69] Driver DM, Seegmiller HL. Features of reattaching turbulent shear layer in divergent channel flow. *AIAA J* 1985;23(2):163–71.
- [70] Papadimitriou C, Lombaert G. The effect of prediction error correlation on optimal sensor placement in structural dynamics. *Mech Syst Signal Process* 2012;28:105–27.
- [71] Bertsekas DP. Nonlinear programming. 2nd ed. Athena Scientific; 1999.